
Chapter 4

Metal nanoparticles stabilized by chiral ligands with carbohydrate backbone

- 4.1** Introduction
 - 4.1.1** Background information on metal nanoparticles
 - 4.1.2** Formation of metal nanoparticles
 - 4.1.3** Methods for characterizing metal nanoparticles
 - 4.1.4** Catalytic applications of metal nanoparticles
 - 4.2** Results and discussion
 - 4.2.1** Synthesis of palladium nanoparticles
 - 4.2.2** Synthesis of ruthenium nanoparticles
 - 4.2.3** Synthesis of rhodium nanoparticles
 - 4.2.4** Application in catalysis of metal nanoparticles
 - 4.3** Conclusions
 - 4.4** Experimental section
 - 4.5** References
-

Abstract. *The synthesis of new metal nanoparticles is reported. Palladium, ruthenium and rhodium nanoparticles have been synthesised following the organometallic approach in the presence of chiral carbohydrate derivative ligands. The shape, size and agglomeration of the nanoparticles depend strongly on the metal precursor and the stabiliser used. We also report the use of rhodium nanoparticles in the styrene hydroformylation reaction that provides low conversions, high regioselectivities and enantioselectivities that are slightly higher than those obtained with an equivalent molecular system.*

4.1 Introduction

4.1.1 Background information on metal nanoparticles

Recently, interest in chemical species of nanometric size has been growing.^[1-17] Inorganic particles in solution, or colloids, as Graham described in 1861 as very slow sedimentation and noncrystalline state^[18], have been known for ages. The first rational synthesis of gold colloids was described by Faraday in 1857.^[19] Since then, many methods to produce particles in solution have been reported.^[1-17]

These species have attracted renewed interest because they have unique properties, somewhere between those of bulk and single-particle species.^[10] For example, if a metal particle with bulk properties is reduced to the size of a few dozen or a few hundred atoms, the density of states in the valence band and the conductivity band, respectively, decreases to such an extent that the electronic properties change dramatically. In fact, the separation between the bands increases when the size of the material decreases.

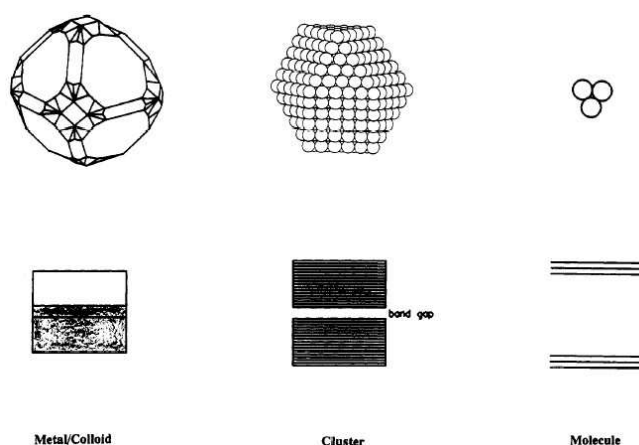


Figure 4.1. Illustration of the electronic states in (a) a metal particle with bulk properties and its typical band structure, (b) a large cluster of cubic close-packed atoms with a small band gap, and (c) a simple triatomic cluster with completely separated bonding and antibonding molecular orbitals^[1]

Three metal atoms, for instance, form energetically well-defined bonding and antibonding molecular orbitals (Figure 4.1c). However, the main point of interest is to be seen in the transition from Figure 4.1a to Figure 4.1b or vice versa. If the number of electronic dimensions in a bulk system is reduced considerably a "quantum dot" (dimension zero) is formed, which corresponds to the nanoparticles or nanoclusters. In the nanoparticles, the quasi-continuous density of states is replaced by a discrete energy level.^[1]

This renewed interest in the intermediate physical and chemical properties of these objects has evidenced that there is a need to control the particles' monodispersity, size, shape, organization and the nature of the chemical species on surface. *Modern* transition-metal nanoclusters differ from *classical* colloids in several important aspects. They are generally: a) smaller (1-10 nm in diameter) than *classical* colloids (>10 nm), b) isolable and redissolvable, unlike *classical* colloids c) soluble in organic solvents (*classical* colloid chemistry is typically aqueous) and d) have a well defined composition. In addition *modern* transition-metal nanoclusters have: e) narrower size dispersions, f) clean surfaces, g) reproducible synthesis and h) reproducible catalytic activities.^[10, 15]

Full-shell ("magic number") metal clusters

Metal clusters which have a complete, regular outer geometry are known as full-shell, or "magic number", clusters (Figure 4.2). Full-shell clusters are constructed by successively packing layers, or shells, of metal atoms around a single metal atom. The total number of metal atoms, per v th shell is given by the equation: $10v^2 + 2$ ($v > 0$).

Thus, the full-shell metal clusters contain a total number of atoms of 13 (1+12), 55 (13+42), 147 (55+92), 309, 561, etc.^[20] Figure 4.2 shows the idealised representation of cubeoctahedron structure full-shell "magic number" clusters. Note that as the number of atoms increases, the percentage of surface atoms decreases.






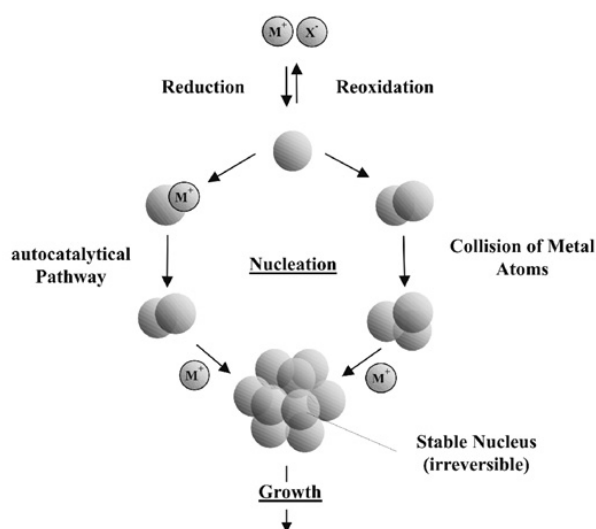
	Number of shells	Atoms present before actual shell	Number of atoms in actual shell ($10n^2+2$)	Total number of atoms in cluster (magic numbers)	Relative amount of surface atoms
	1	1	12	13	92%
	2	13	42	55	76%
	3	55	92	147	63%
	4	147	162	309	52%
	5	309	252	561	45%

Figure 4.2. Idealised representation of the cubeoctahedron structure of full-shell “magic number” clusters. Each atom has the maximum number of nearest neighbours, which impart some degree of extra stability to full-shell clusters.^[4]

Mechanistic studies of nanocluster formation and growth

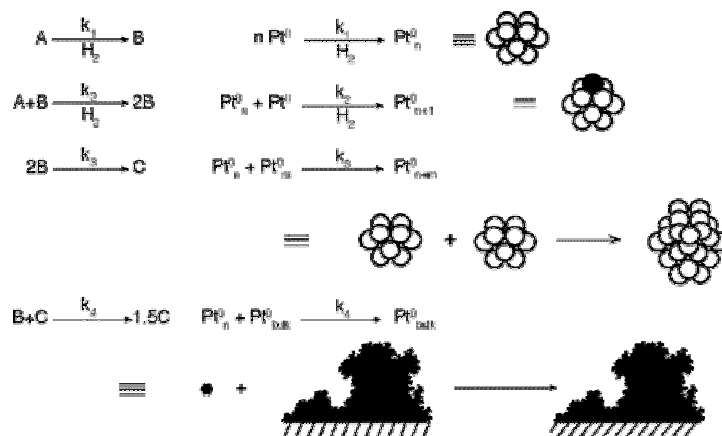
Turkevich et al.^[21-23] proposed the first reproducible standard protocols for preparing metal colloids (e.g. the reduction of $[\text{AuCl}_4]_2$ with sodium citrate). They also proposed the mechanism for the formation of nanoclusters that consist of nucleation, growth and agglomeration. This proposed mechanism, refined by more recent thermodynamic and kinetic results,^[24-27] is presented in Scheme 4.1.

First, the metal salt is reduced to give zerovalent metal atoms, which can collide in solution with metal ions, metal atoms or clusters, to form an irreversible stable nuclei. The diameter of the nuclei depends on the strength of the metal-metal bonds and the difference between the redox potentials of the metal salt and the reducing agent applied.^[12]



Scheme 4.1. Formation of nanostructured metal colloids by reduction of metal salts^[12]

Finke et al. proposed a new mechanism for the formation of transition metal nanoclusters.^[28-32] They used hydrogen as reducing agent to study iridium(0) clusters, and proposed a three-step mechanism consisting of a slow and continuous nucleation step, followed by a fast autocatalytic surface growth and then a bimolecular agglomeration step. The autocatalytic growth of the surface begins after the formation of Ir(0)_n nuclei with a small size but critique (n). When the cluster reaches a size of the "magic number" gains a thermodynamic stability associated to a full-shell metal cluster. The nanocluster increases its stability because the surface atoms have the maximum metal-metal bonds. Recently, Finke et al.^[33, 34] proposed a more general four-step mechanism involving double autocatalysis (Scheme 4.2). These studies were performed with platinum(0) clusters and hydrogen as reducing agent. The mechanism consists of: 1) a slow continuous nucleation, 2) fast autocatalytic surface growth, 3) bimolecular agglomeration and 4) an autocatalytic agglomeration step between small and large, bulk-metal-like particles.



Scheme 4.2. Proposed four-step, double autocatalytic mechanism in graphic form^[33]

4.1.2 Formation of transition-metal nanoparticles

4.1.2.1 Stabilisation of transition-metal nanoparticles

The metal particles are unstable with respect to the agglomeration to the bulk. The agglomeration is an undesired process because it leads to the loss of the properties associated with the colloidal state of the metal particles. The stability of these particles results from the equilibrium of the van der Waals attractive forces and the electrostatic repulsive forces. In the absence of repulsive forces opposed to van der Waals forces the colloidal metal particles will aggregate. Thus a stabilising agent is needed to provide stable nanoparticles. There are two general kinds of stabilisation procedures: 1) electrostatic stabilisation by the surface adsorbed anions and 2) steric stabilisation by the presence of bulky groups. The combination of these two kinds of stabilisation lead to 3) electrosteric stabilisation.^[14]

Electrostatic stabilisation

The electrical double-layer around the particle consisting of adsorbed ions on the surface (dissolved halides, carboxylates or polyoxianions, generally aqueous) and their respective counterions (Figure 4.3) generates a Coulombic repulsion between

the particles. If the associated electrical potential is high enough, then the electrostatic repulsion prevents the aggregation. However, the electrostatic stabilisation can be strongly influenced by various factors, such as a thermal or ionic strength change, which can modify the electrical double-layer.^[10, 14, 35-37]

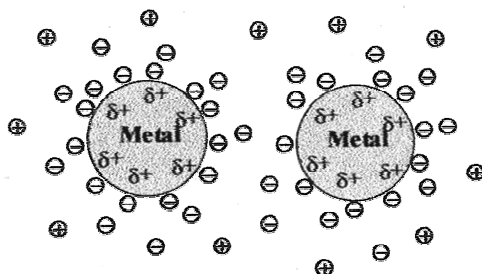


Figure 4.3. Schematic representation of electrostatic stabilisation of metal colloid particles^[14]

Steric stabilisation

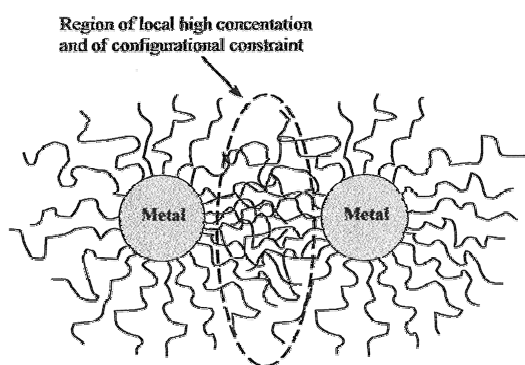


Figure 4.4. Schematic representation of steric stabilisation of metal colloid particles^[14]

The adsorption of molecules, such as polymers or oligomers, at the surface of the particle provides a protective layer. This layer prevents aggregation in two ways: 1) in the interparticle space (Figure 4.4), movement is restricted which decreases the entropy and, thus, increases the free energy; and 2) the concentration of these molecules in the interparticle space is high and the solvent re-establishes the

equilibrium by diluting the macromolecules and thus separating the particles. Steric stabilisation is used in both organic and aqueous media, while electrostatic stabilisation is mainly used in aqueous media. However, the properties of the macromolecules, length or composition, can have a strong influence on the stability of the particles.^[14, 36, 38]

Electrosteric stabilisation

Ionic surfactants provide a stabilisation which combines electrostatic and steric stabilisation. These compounds have a polar group that can generate an electrostatic stabilisation, and a lipophilic side chain that can provide steric repulsion.^[39-42] Compounds such as $(\text{Bu}_4\text{N}^+)/(\text{P}_2\text{W}_{15}\text{Nb}_3\text{O}_{62}^{9-})$, which combines bulky ammonium counteranions with a highly charged polyoxoanion, provide an efficient electrosteric stability toward the agglomeration (Figure 4.5).^[10, 40]

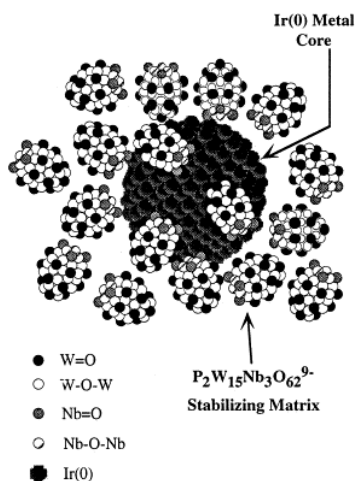
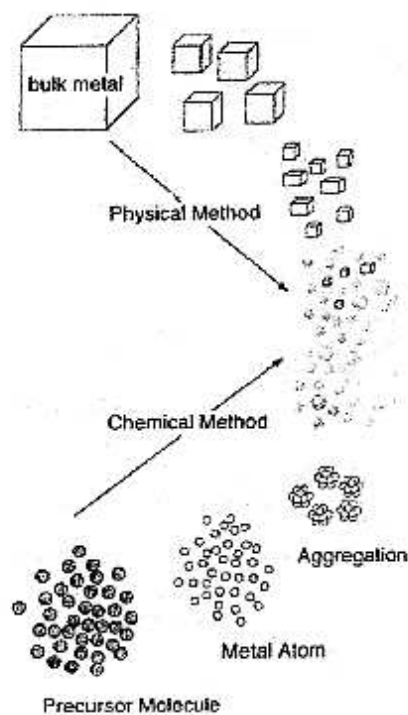


Figure 4.5. Idealized, roughly-to-scale representation of a $\text{P}_2\text{W}_{15}\text{Nb}_3\text{O}_{62}^{9-}$ polyoxoanion and Bu_4N^+ stabilized $20 \pm 3 \text{ \AA}$ $\text{Ir}(0)_{\sim 300}$ nanocluster, $[\text{Ir}(0)_{\sim 300} (\text{P}_4\text{W}_{30}\text{Nb}_6\text{O}_{123}^{16-})_{\sim 33}] (\text{Bu}_4\text{N})_{\sim 300} \text{Na}_{\sim 228}$. For the sake of clarity, only 17 of the polyoxoanions are shown, and the polyoxoanion is shown in its monomeric, $\text{P}_2\text{W}_{15}\text{Nb}_3\text{O}_{62}^{9-}$ form (and not as its Nb–O–Nb bridged, anhydride, $\text{P}_4\text{W}_{30}\text{Nb}_6\text{O}_{123}^{16-}$ form). The $\sim 330 \text{ Bu}_4\text{N}^+$ and $\sim 228 \text{ Na}^+$ cations have also been omitted, again for the sake of clarity.^[39]

4.1.2.2 Synthesis of transition-metal nanoparticles

Dispersions of metallic nanoparticles can be obtained by two main methods: mechanic subdivision of metallic aggregates (physical method) or nucleation and growth of metallic atoms (chemical method) (Scheme 4.3). The chemical methods provides metal nanoparticles with greater control of shape, size, surface, composition and reproducibility than physical methods.



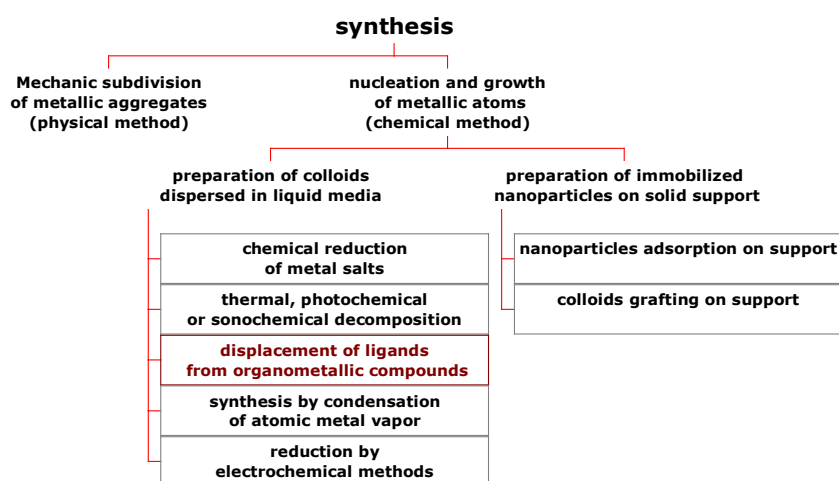
Scheme 4.3. Schematic illustration of preparative methods of metal nanoparticles^[15]

The colloids synthesised by chemical methods can be dispersed in liquid media or immobilised on a solid support. The literature describes five main general methods for synthesizing transition-metal colloids (Scheme 4.4): 1) chemical reduction of metal salts, 2) thermal, photochemical or sonochemical decomposition, 3)

electrochemical reduction, 4) metal vapor synthesis and 5) ligand reduction and displacement from organometallic complexes.

The chemical reduction of metal salts

This is the most widely used method for synthesizing metal colloids. Several reducing agents have been used: for example molecular hydrogen or carbon monoxide, hydrides or salts such as sodium borohydride, or oxidable agents such as alcohols. The most commonly used stabilising agents are polymers such as PVP (polyvinylpyrrolidone), PVA (polyvinyl alcohol) or PVE (polyvinyl ether) and dendrimers such as PAMAM (polyamidoamine).^[14]



Scheme 4.4. Methods for synthesizing metal nanoparticles

Thermal, photochemical or sonochemical decomposition

This method consists in the decomposition of transition metal salts or organometallic complexes to their respective zerovalent element by thermolysis (by application of heat),^[14, 43, 44] photolysis (by ionisation radiations or UV-Visible irradiation)^[14, 26, 45-48] or sonochemical reduction (by application of ultrasounds).^[49-51]

Metal vapour synthesis

Metal vapour synthesis consists of evaporating relatively volatile metals at reduced pressure and subsequently co-condensing them at low temperatures with the vapours of organic solvents. The colloidal particles nucleate and grow as the frozen mixture warms to melting.^[14, 52, 53]

Electrochemical reduction

Recently Reetz et al.^[14, 54-56] developed the electrochemical method which consists in the dissolution of the anode to form metal atoms. These are then reduced on the cathode to form particles after the aggregation, in the presence of ammonium salts which are both electrolyte and stabilising agent.

Ligand reduction and displacement from organometallics

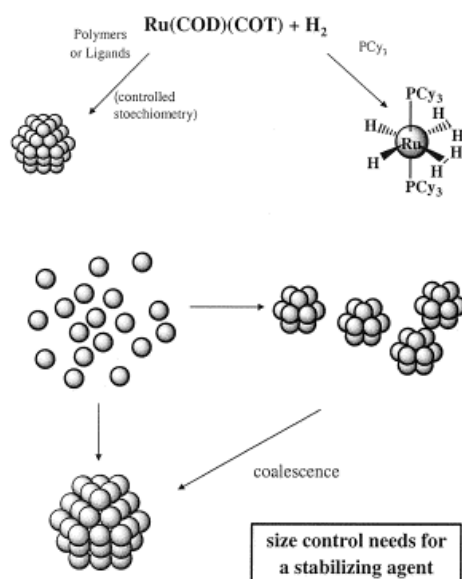
The synthesis procedure consists of decomposing an organometallic precursor, mainly zerovalent organometallic complexes, in an organic solvent. This method makes it possible to synthesise nanoparticles with clean surface, because not reductive chemical agents are used. In other methods of synthesis, the impurities generated, such as salts or water, are in contact with the surface and are difficult to remove, so they modify the properties of the nanoparticles.

The rhodium precursor $[\text{Rh}_2(\mu\text{-Cl})_2(\text{CO})_4]$ was decomposed under hydrogen to form small rhodium nanoparticles (1.5-2.5 nm).^[57] Finke et al.^[39, 58] used iridium and rhodium organometallic complexes to synthesise, under hydrogen, stable and monodisperse nanoparticles. $\text{Fe}(\text{CO})_5$ was used to synthesise nanoparticles in anisole in the presence of PPO (poly(dimethylphenylene oxide)) as stabilisers by sonolysis.^[59]

Bradley and co-workers synthesised platinum nanoparticles that were stabilised with PVP by using molecular hydrogen to reduce $[\text{Pt}(\text{dba})_2]$ ^[60] and $[\text{Pt}_2(\text{dba})_3]$.^[61] (dba: dibenzylidene acetone) Palladium and platinum nanoparticles were also

synthesised from $[\text{Pd}(\text{dba})_2]$ and $[\text{Pt}(\text{dba})_2]$ using CO in the presence of cellulose acetate or cellulose nitrate in THF.^[62, 63]

The organometallic approach to nanoparticles synthesis developed by Chaudret and co-workers^[14, 16, 17] make it possible to synthesise metal nanoparticles in mild conditions and control the size, shape and surface environment. This procedure consists in the decomposition of an organometallic precursor able to decompose in mild conditions, generally using a reducing gas, hydrogen or carbon monoxide (Scheme 4.5). The ideal precursor is a zerovalent olefinic complex, which leads to the production of an alkane unable to form strong bonds with the growing metal surface in these conditions. Precursors of this type are $[\text{Ni}(\text{C}_8\text{H}_{12})]$ ^[64] and $[\text{Ru}(\text{C}_8\text{H}_{10})(\text{C}_8\text{H}_{12})]$,^[65, 66] which both decompose under hydrogen in mild conditions. Such metal precursors as $[\text{Co}(\text{C}_8\text{H}_{13})(\text{C}_8\text{H}_{12})]$ ^[67, 68] or $[\text{Rh}(\eta^3\text{-C}_3\text{H}_5)_3]$,^[69, 70] with allylic groups, which decompose easily in these mild conditions, have also been used. However, when olefinic precursors are not available other complexes have been used. $[\text{Pd}(\text{dba})_2]$, $[\text{Pt}(\text{dba})_2]$ ^[59] or $[\text{Rh}(\text{acac})(\text{C}_8\text{H}_{12})]$,^[69, 71] for example, also decompose in mild conditions, but release potential ligands can perturb the surface.



Scheme 4.5. Illustration of the general synthetic method for the synthesis of metal nanoparticles followed by Chaudret and co-workers^[16]

The nanoparticles synthesised by the organometallic approach were stabilised with polymers, solvents or ligands. Polymers, such as PVP or cellulose acetate, were used as stabilisers in the synthesis of ruthenium,^[62, 65, 72] platinum,^[73] nickel,^[64] cobalt^[74] and bimetallic nanoparticles.^[72, 74, 75] However, in this synthesis a polymer is not required to stabilize the particles. This method have been used to synthesise nanoparticles stabilised by solvents. [Pt(dba)₂] reacts with carbon monoxide in THF to give a colloid containing fcc (face-centered cubic) particles with a mean size of 1.2 nm and a narrow size distribution.^[59] The synthesis of ruthenium nanoparticles from [Ru(C₈H₁₀)(C₈H₁₂)] with H₂ in THF, or non coordinating solvents, leads to the precipitation of ruthenium powder.^[66, 76] However, when alcohols were used as solvent, colloidal solutions with ruthenium nanoparticles were obtained. In synthesis carried out in THF/MeOH mixtures, a correlation was found between the size of the particles obtained and the THF/MeOH ratio (Figure 4.6).^[76]

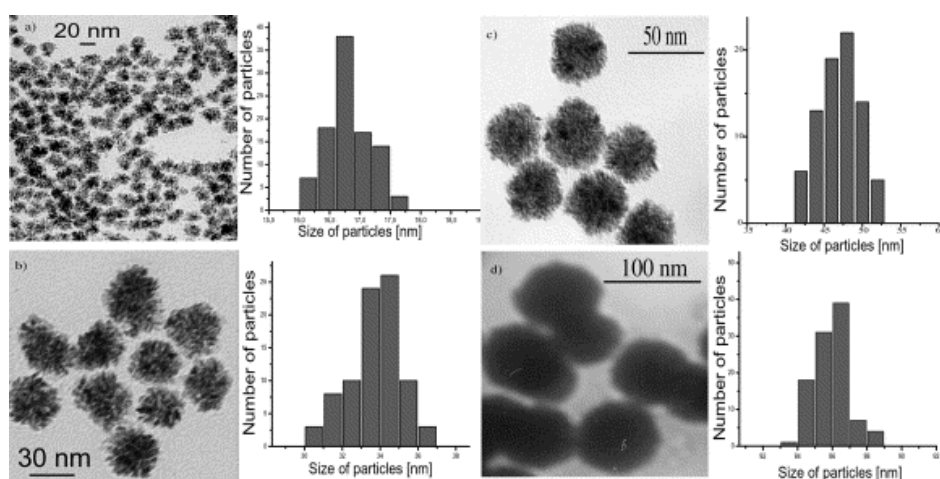


Figure 4.6. TEM Micrographs and histograms of the size of ruthenium nanoparticles synthesized in different MeOH/THF mixtures (a: MeOH/THF = 5/95; b: MeOH/THF = 25/75; c: MeOH/THF = 50/50; d: MeOH/THF = 90/10).^[16, 76]

Ligand-protected nanoparticles can also be synthesised by this method, usually the synthesis are carried out in the presence of substoichiometric quantity of ligand. Monodentate ligands, such as PPh₃, thiophenols, long-chain thiols or amines, have been used to synthesise different metal nanoparticles.^[16] Bidentate ligands have

also been used to stabilise metal nanoparticles by this method, for instance, a diphosphine ligand such as bis(diphenylphosphino)decane.^[77] These makes it possible to use nanoparticles in asymmetric catalysis when the metal nanoparticles are stabilised with chiral ligands. Chiral oxazoline or amino alcohol ligands have been used to stabilize palladium and ruthenium nanoparticles.^[78] In both cases, the ligands provide an excellent stabilisation of the particles, which can be handled like molecular species. Diphosphite chiral ligands were also used as stabilisers of palladium nanoparticles.^[79] These palladium nanoparticles were active in the asymmetric allylic alkylation, providing excellent enantioselectivities and kinetic resolution of the substrate.

4.1.3 Methods for characterizing metal nanoparticles

The key goal of nanoparticles characterisation is to establish their size, structure and general composition. The techniques that are most often used to characterise nanoparticles are summarised in Figure 4.7. Nanoparticles can be characterised both by techniques that are common in the field of nanomaterials (TEM, SEM, XRD etc.) and by techniques derived from molecular chemistry (spectroscopies:IR, UV, NMR; magnetic measurements).

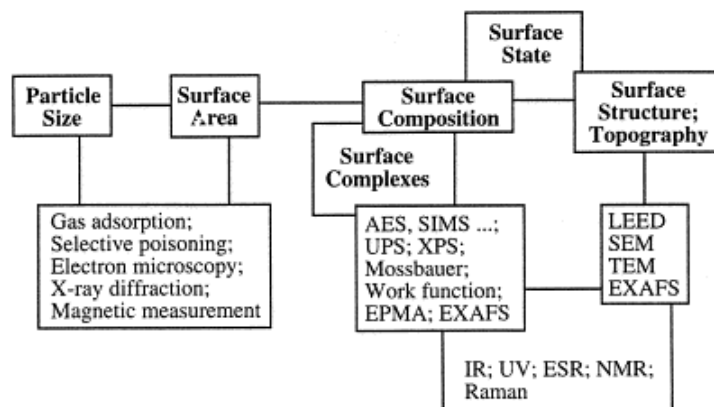


Figure 4.7. Common methods available for the characterisation of nanoparticles^[10]

Transmission electron microscopy

Transmission electron microscopy (TEM) or high resolution TEM are the most widely used techniques for characterizing metal nanoparticles. These techniques provide direct visual information about size, shape, dispersity, structure and morphology. TEM has routine magnifications of ≥ 100000 with a resolution of $\pm 4 \text{ \AA}$ and HRTEM have a routine magnifications of ≥ 1000000 with a resolution of $\pm 2 \text{ \AA}$. The disadvantages of these techniques are: 1) electron beam induces structural rearrangement, aggregation or decomposition of the nanoparticles, 2) three-dimensional samples must be interpreted from two-dimensional images and 3) the samples are dried and examined under high-vacuum condition, so no direct information of nanoparticles in solution is obtained.^[10]

Infrared spectroscopy

Infrared spectroscopy (IR) has been used to study the surface of nanoparticles and the adsorption of molecules on the surface. Carbon monoxide has been widely used as a ligand because it easily adsorbs on metal surfaces and has a characteristic vibrational frequencies around $1800\text{-}2100 \text{ cm}^{-1}$.^[3, 16, 17]

X-ray diffraction

X-ray diffraction is a non destructive technique which can identify the crystal phase for particles larger than 3 nm. When the nanoparticles are smaller, the acquisition of structural information is more difficult.^[61] More sophisticated techniques such as EXAFS (Extended X-ray Absorption Fine Structure), to determine the atomic number, distance and coordination number of the atoms surrounding the element whose absorption edge is being examined, can also be employed.

Wide angle X-Ray Scattering

Wide angle X-Ray Scattering (WAXS) is an X-ray diffraction technique that is often used to determine the crystalline structure. This technique specifically analyses of Bragg Peaks scattered to wide angles, which (by Bragg's law) implies that they are

caused by small structures. The samples are analysed in solid state, sealed in 1mm Lindemann glass capillaries. The diffused corrected intensity is due to: 1) chemical composition of the nanoparticles, 2) structure of the nanoparticles and 3) interactions between the nanoparticles. The radial distribution function is obtained by the Fourier transform of the intensity, and facilitates interpretation. The WAXS provides a distribution of the metal-metal bonds inside a homogeneous assembly of nanoparticles, since well-defined RDF indicates well-crystallised nanoparticles. Using a model is then possible to have an access to the structure of the particle and to its coherence length, assuming that all particles adopt the same size and structure (Figure 4.8 shows an example of a Radial distribution function (RDF) obtained from WAXS analysis).

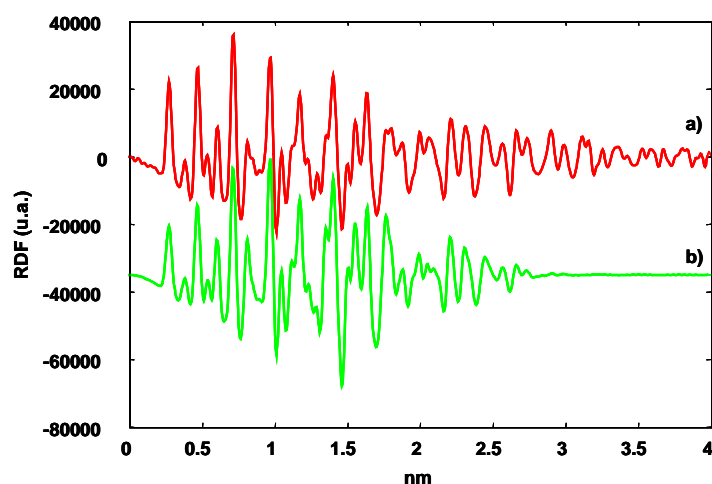


Figure 4.8. Radial distribution function (RDF) obtained from WAXS analysis. Comparison between a) experimental results of rhodium nanoparticles stabilised with diphosphite ligand and b) theoretical RDF of spherical rhodium nanoparticles with fcc structure and 3 nm of diameter.

Nuclear magnetic resonance

The NMR of metal nanoparticles can provide two sorts of information: about the ligands that surround the metal core and about the intra-core metallic atoms. NMR studies of the metal core are typically more difficult because the nuclear-spin lattice

relaxation time, and the nuclear resonance itself, are sensitive to any metallic property the cluster may exhibit. The NMR of ligand-protected nanoparticles is little developed, however, several recent studies demonstrate that it is possible to observe long chain ligands ligated to metal particles by ^1H and ^{13}C NMR spectroscopy. In this case, the nuclei close to the metal surface are not visible because of the slow tumbling of the metal particle in solution.^[16, 65]

4.1.4 Catalytic applications of metal nanoparticles

Recently, interest in the catalytic properties of transition metal colloids has been growing. This is due to the very large specific surface of the metal nanoparticles, consequently a large number of metal atoms are available to the substrates.^[14] Metal nanoparticles have been proven to be efficient and selective catalysts for reactions which are also catalysed by molecular complexes such as olefin hydrogenation or C-C coupling, as well as for reactions which are not or poorly catalysed by molecular species such as aromatic hydrocarbons hydrogenation.^[10-12, 14, 15, 80, 81] Recently, metal nanoparticles have been applied to enantioselective catalyst for reactions such as hydrogenation^[82-87] or allylic alkylation.^[79]

4.1.4.1 Hydrogenation catalysed by metal nanoparticles

Hydrogenation of olefins (terminal, internal or cyclic) and benzene derivatives have been widely studied with transition metal nanoparticles as catalysts. In this kind of reactions, transition metal nanoparticles showed good activities and selectivities.^[14, 15]

Cinnamaldehyde was hydrogenated to cinnamic alcohol by Liu et al. High selectivities to the alcohol were obtained using several metal and bimetallic colloids such as Pt, Pt/Co in PVP or Pt immobilised in supports such as polystyrene or alumina.^[88] Chloronitrobenzenes (*ortho*-, *para*- or *meta*-) were successfully hydrogenated to the corresponding chloroanilines with Pd/PVP, Pt/PVP and Ru/PVP systems.^[89, 90] The hydrogenation of other substrates such as 1,5-cyclooctadiene,^[91] citronelal^[92] or ketones^[93] have also been studied with colloidal systems.

Nevertheless, the most studied reaction is the hydrogenation of arene derivatives. Arene hydrogenation is an important industrial catalytic transformation. Generally heterogeneous catalysts have been used in this reaction but homogeneous systems have also been reported.^[10, 14] However, in recent years the application of colloidal systems in arene hydrogenation has increased dramatically. Rhodium is the most frequently used metal, followed by ruthenium. They both showed high activities in heterogeneous catalysis. The most commonly used precursors are $[\text{Rh}(\mu\text{-Cl})(\text{diene})]_2$, $\text{RhCl}_3 \cdot \text{H}_2\text{O}$ and $\text{RuCl}_3 \cdot \text{H}_2\text{O}$ and the most commonly used stabilisers are tetraalkylammonium salts. Generally, the catalysis is biphasic (aqueous/organic) and takes place in mild reaction conditions (room temperature and 1 atm H_2).^[15] The hydrogenation of arenes with two or more substituents on the benzene ring produces *cis* or *trans* diastereoisomers, and the metal nanoparticles favour the thermodynamically less favourable *cis* diastereoisomer. Enantioselective hydrogenation is possible when multisubstituted arenes are hydrogenated.

Finke et al.^[94] reported the use of Rh(0) nanoparticles in arene hydrogenation. The nanoparticles were formed *in situ* by reducing $[\text{Bu}_4\text{N}]_5\text{Na}_3[(1\text{-5-COD})\text{Rh} \cdot \text{P}_2\text{W}_{15}\text{Nb}_3\text{O}_{62}]$ with H_2 , and they showed high activities and selectivities in anisole hydrogenation.

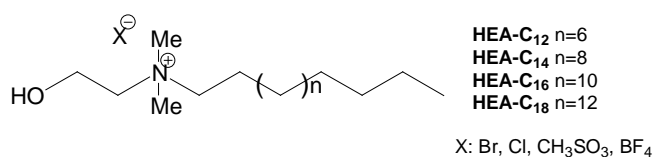


Figure 4.9. N-alkyl-N-(2-hydroxyethyl)ammonium salts, HEA-Cn-X^[95, 96]

Roucoux and co-workers have also reported the hydrogenation of arenes with metal nanoparticles. Rhodium nanoparticles were synthesised by reducing $\text{RhCl}_3 \cdot 3\text{H}_2\text{O}$ with sodium borohydride and stabilised with various surfactants, (N-alkyl_n-N-(2-hydroxyethyl)ammonium salts HEA-Cn-X (Figure 4.9), and were successfully used in biphasic arene hydrogenation. The catalytic systems were efficient under mild conditions (room temperature and 1 atm H_2 pressure). The aqueous phase which contains the protected rhodium(0) colloids were reused without a significant loss of

activity.^[41, 95, 97] These authors also observed that the nature of the surfactant counteranion has a strong influence on the catalyst results, the best results were obtained when chloride was used as counteranion.^[96] Various heterocyclic aromatic compounds were also hydrogenated with rhodium nanoparticles stabilised with this kind of surfactants.^[98] Iridium nanoparticles synthesised from IrCl₃ by the same method in the presence of HEA-16-Cl showed high activities and selectivities in arene hydrogenation.^[99]

Dupont et al. synthesised stable transition-metal nanoparticles of the type [M⁰]_n (M: Ir^[100, 101], Rh^[100, 101], Pt^[100] and Ru^[101, 102]) by reducing the corresponding metal precursors dissolved in 1-*n*-butyl-3-methylimidazolium (BMI) hexafluorophosphate ionic liquid (Figure 4.10) by molecular hydrogen. The isolated [M⁰]_n nanoparticles were redispersed in the ionic liquid or in various solvents or they were used in solventless conditions for the liquid-liquid biphasic, homogeneous or heterogeneous hydrogenation of arenes under mild reaction conditions (75°C and 4 atm H₂). The recovered metal nanoparticles were reused several times without any significant loss in catalytic activity.

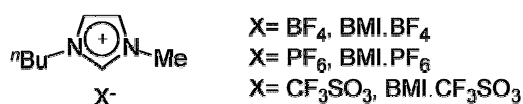


Figure 4.10. Imidazolium room temperature ionic liquids^[103]

4.1.4.2 C-C coupling reactions catalysed by metal nanoparticles

C-C coupling reactions, such as Heck or Suzuki couplings, have been catalysed by metal nanoparticles.^[14] The most common metal used is palladium. Reetz and co-workers^[104] described the use of palladium nanoparticles, synthesised by the electrochemical process (see above), in the Heck coupling reaction. The same authors also used Pd and Pd/Ni nanoparticles in Suzuki coupling reactions, and the bimetallic colloid showed the best activities.^[105] Titanium^[106] and nickel^[107] nanoparticles were also synthesised by the same method and successfully applied to olefin-forming McMurry-type coupling of aldehydes and ketones, and to the 3+2 cycloaddition reactions, respectively.

El-Sayed and co-workers have used palladium^[108-113] and platinum^[114] nanoparticles, stabilised with various stabilisers such as dendrimers (PAMAM) or polymers (PVP and others), in Suzuki coupling reactions. They have investigated how the characteristics of the nanoparticles (size, shape or stability) affect catalytic activity.^[115]

Dupont and co-workers^[116] have also used palladium nanoparticles dispersed in ionic liquid BMI.PF₆ (Figure 4.10, see above) to investigate the Heck reaction. These Pd(0) nanoparticles with 2 nm diameter were efficient catalyst precursors for coupling of aryl halides with *n*-butylacrylate. *In situ* TEM analysis of the ionic liquid catalytic solution after the catalytic reaction showed the formation of larger nanoparticles (6 nm). It was also observed significant metal leaching (up 34%) from the ionic phase to the organic phase at low substrate conversions and drops to 5-8% leaching at higher conversions. These results strongly suggest that the Pd(0) nanoparticles serve as a reservoir of "homogeneous" catalytic active species.

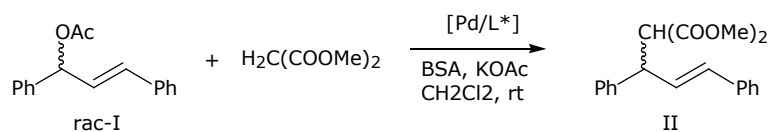
4.1.4.3 Enantioselective reactions catalysed by metal nanoparticles

Metal nanoparticles have been proven to be efficient and selective catalysts for reactions such as olefin hydrogenation or C-C coupling reactions. However, despite impressive progress in asymmetric catalysis, the use of metal nanoparticles as enantioselective catalysts is not very widespread. The first example was reported by Lemaire and co-workers.^[117] Rhodium nanoparticles stabilised with a chiral amine were used in the hydrogenation of disubstituted arenes but the enantioselectivities were poor.

The most studied enantioselective reaction catalysed by metal colloids is the hydrogenation of ethyl pyruvate. Bönnemann^[83, 85] studied this reaction with platinum colloids stabilised with dihydrocinchonidine salt. They obtained enantioselectivities of 75-80% in (*R*)-ethyl lactate. Platinum nanoparticles stabilised by PVP and modified with cinchonidine were also tested in this reaction, and showed enantioselectivities of 95-98% (*R*).^[82, 84, 118] Recently, Roucoux and co-workers,^[119] described the biphasic version of this reaction. The aqueous phase containing the Pt(0) nanocatalysts was used for further runs with a total

conservation of activity and enantioselectivity for (*R*)-ethyl lactate up to 55%. Similar systems based on rhodium^[120] and iridium^[121] nanoparticles, stabilised with PVP and modified with cinchonidine, have also been described, the enantioselectivities obtained were lower than with palladium- and platinum- based systems.

Recently, palladium nanoparticles synthesised by the organometallic approach^[16, 17] have been applied to the asymmetric allylic alkylation of *rac*-3-acetoxy-1,3-diphenyl-1-propene with dimethyl malonate (Scheme 4.6).^[79]



Scheme 4.6. Asymmetric allylic alkylation of *rac*-3-acetoxy-1,3-diphenyl-1-propene with dimethyl malonate

The palladium nanoparticles, **Colloid.1**, were synthesised by decomposing $[\text{Pd}_2(\text{dba})_3]$ by H_2 (3 bar) at room temperature in THF in the presence of diphosphite ligand **1** (Figure 4.11). These palladium nanoparticles behaved as efficient kinetic resolution catalyst giving >95% of enantiomeric excess in II and 89% of enantiomeric excess in the remaining substrate I at 56% of conversion (Scheme 4.6).

One of the problematic point of the application of metal nanoparticles in catalysis is to know the true nature of the catalysis, colloidal or molecular. In this study the authors observed that the reactions using the two different catalytic systems, colloidal system and the respective molecular system, displayed some clear differences, the most notable ones being the absence of completion of the reaction associated to a very high kinetic resolution when using **Coll.1** as a catalyst. In contrast, quasi total conversion but no kinetic resolution of the substrate was observed using the respective molecular system as the catalyst. The authors carried out several experiments, such as kinetic studies, comparison of the colloidal system with diluted molecular systems or poisoning test, among others, to rule out

the possibility of the formation from the particles of a small amount of an active molecular catalyst. With this studies they demonstrated that two different mechanisms operate according to the nature of the catalyst.

Objective

With these previous results we decided to synthesise new palladium nanoparticles from the same palladium precursor, $[\text{Pd}_2(\text{dba})_3]$, stabilised with diphosphites **2** and **3**, and with phosphine-phosphite ligand **4** (Figure 4.11), in order to compare the effect of the ligand on the stabilisation and the characteristics of the nanoparticles. We also extended this method to synthesise other metal nanoparticles, ruthenium and rhodium, stabilised with carbohydrate derivative ligands (Figure 4.11) in order to compare the effect of the metal precursor and the stabiliser used, on the nanoparticles synthesised. Palladium nanoparticles synthesised in the presence of chiral ligands **1**, **2**, **3** and **4** were applied in the palladium-catalysed allylic alkylation as catalyst. Rhodium colloids synthesised in the presence of chiral ligands **1** and **3** were used as catalyst in the hydroformylation of styrene.

4.2 Results and discussion

The synthesis of nanoparticles through the organometallic approach was developed by Chaudret and co-workers.^[16, 17] It makes it possible to synthesize nanoparticles of uniform small size (1–3 nm) and clean surface, and it consists in the decomposition of an organometallic precursor, preferably a zerovalent olefinic precursor, able to decompose in mild conditions, generally with a reducing gas, such as hydrogen or carbon monoxide, in the presence polymers or ligands in sub-stoichiometric amounts.

Among the different ligands used to stabilise nanoparticles, such as oxazolines,^[78] phosphines,^[77] etc.,^[16, 17] diphosphite ligands (Figure 4.11) are interesting for stabilising metal nanoparticles because they have phosphorus and oxygen atoms, that can interact, strongly and weakly, respectively, with the surface. As has been mentioned above, palladium nanoparticles synthesised by the organometallic approach and stabilised with chiral xylofuranoside diphosphite **1** (Figure 4.11) have

been previously described.^[79] In order to study how of the skeleton and the phosphorus moieties of the ligands influenced the stabilisation and characterisation of the nanoparticles, we have synthesised a new series of palladium nanoparticles stabilised with diphosphite ligands **2** and **3** and with phosphine-phosphite ligand **4** (Figure 4.11). Ruthenium nanoparticles were prepared from $[\text{Ru}(\text{C}_8\text{H}_{10})(\text{C}_8\text{H}_{12})]$ and rhodium nanoparticles were synthesised from two different rhodium precursor, $[\text{Rh}(\eta^3\text{-C}_3\text{H}_5)_3]$ and $[\text{Rh}(\mu\text{-OMe})(\text{COD})]_2$ in the presence of diphosphite ligands **1** and **3**. Phosphorus chiral ligands derived from carbohydrates **1**^[122], **2**^[123], **3**^[124] and **4**^[125], were prepared by methods described previously.

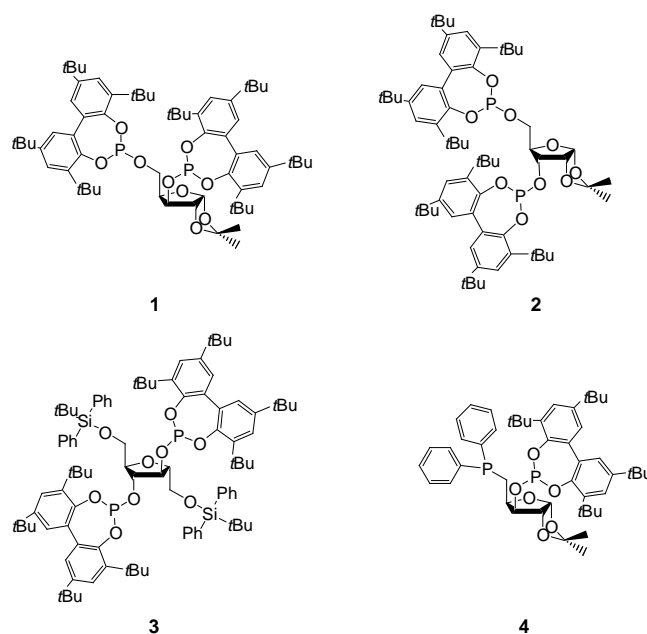


Figure 4.11. Phosphorus chiral ligands derived from carbohydrates

4.2.1 Synthesis of palladium nanoparticles from the precursor $[\text{Pd}_2(\text{dba})_3]$

Palladium nanoparticles stabilised with diphosphite ligand **1**, **Colloid.1**, have been previously described.^[79] These nanoparticles were synthesised by the organometallic approach from the precursor $[\text{Pd}_2(\text{dba})_3]$ following the reaction presented in Scheme 4.7 with a Pd/L ratio of 1/0.2. Transmission electron microscopy revealed the presence of small, elongated, but in some cases

agglomerated, particles with a mean size of ca. 4 nm (Figure 4.12), while Wide-angle X-ray scattering analyses showed the fcc structure of bulk palladium.

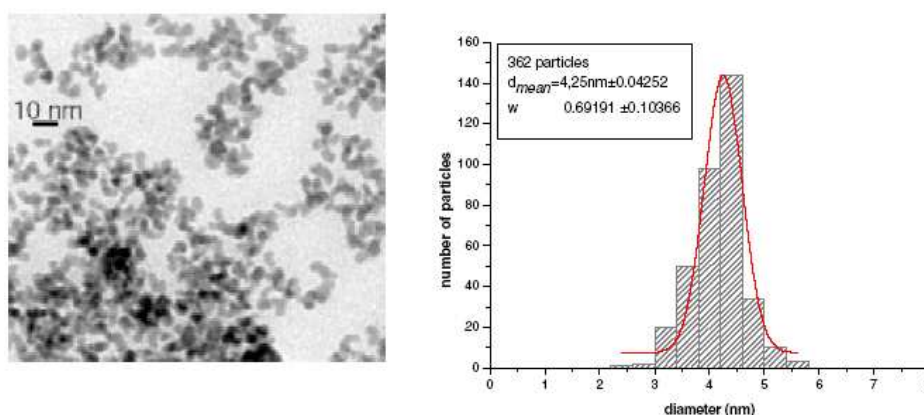
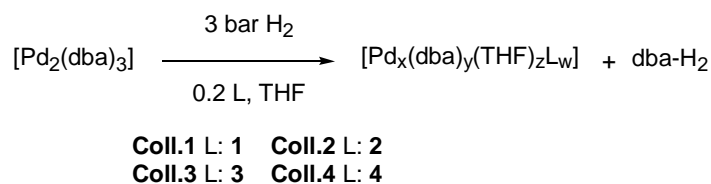


Figure 4.12. Transmission electron micrograph of **Coll.1** and size histogram built from ca. 360 nanoparticles

The synthesis of palladium nanoparticles from the precursor $[\text{Pd}_2(\text{dba})_3]$ was carried out following the reaction presented in Scheme 4.7. Diphosphite ligands **2** and **3** and phosphine-phosphite ligand **4** have been used as stabilisers.



Scheme 4.7. Synthesis of palladium nanoparticles from $[\text{Pd}_2(\text{dba})_3]$ in the presence of chiral ligands **2**, **3** and **4**

The initial THF solution of the palladium precursor in the presence of the ligand was purple red. After pressurization at room temperature under 3 bars of hydrogen for 30 minutes, the solution became black in a few minutes. The nanoparticles were isolated by precipitation with pentane. The nanoparticles synthesised were analysed by TEM (Transmission electron microscopy), WAXS (Wide-angle X-ray scattering) and elemental analysis. The samples for microscopy analysis were prepared from a

drop of the colloidal solution, which was deposited under argon on a holey carbon covered copper grid. The samples for WAXS analysis were prepared from the isolated nanoparticles, which were sealed in 1mm Lindemann glass capillaries.

First, we synthesised palladium nanoparticles with diphosphite chiral ligand **2** as stabiliser, **Colloid.2**. The diphosphite **2**, with C_1 -symmetry differs of the previously used diphosphite **1** only in the configuration of C-3 of the sugar backbone (Figure 4.11). Figure 4.13 shows the nanoparticles synthesised with a palladium/diphosphite ratio of 1/0.2, **Colloid.2**. The elemental analysis of the black isolated nanoparticles of **Colloid.2** was 72.97 %Pd, 0.37%P, 13.99%C, 0.38%H, which displays a Pd/P ratio of 57/1. We observed nanoparticles similar to those described for **Colloid.1**, stabilised with diphosphite **1**. The TEM micrograph revealed small nanoparticles with a mean diameter ca. 4 nm, which are in some cases agglomerated. The WAXS analyses for **Colloid.2** showed the fcc structure of bulk palladium with a coherence length between 3.5 and 4 nm, which is in good accordance with TEM observations.

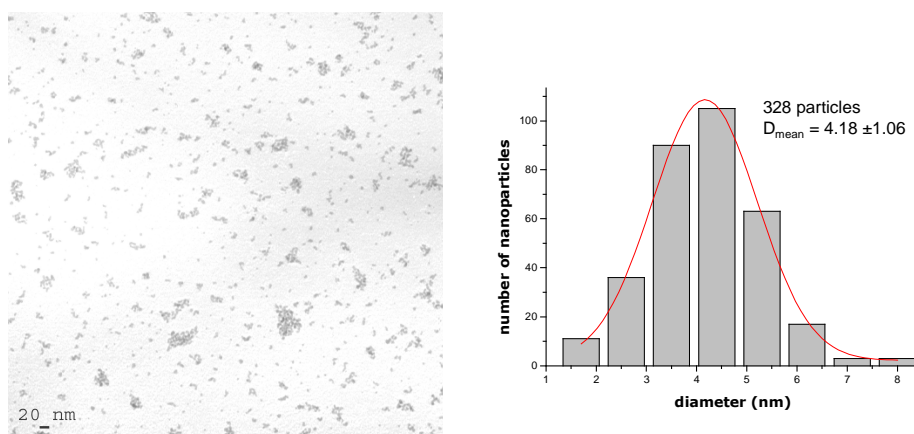


Figure 4.13. Transmission electron micrograph of **Coll.2** and size histogram built from ca. 330 nanoparticles

We also prepared palladium nanoparticles, namely **Colloid.3**, stabilised with diphosphite ligand **3**, which is a new diphosphite ligand with C_2 -symmetry previously described in Chapter 2. The elemental analysis of the black isolated

nanoparticles of **Colloid.3** was 68.77 %Pd, 0.33%P, 2.93%Si, 8.82%C, 0.65%H, which displays a Pd/P ratio of 60/1, similar to that in **Colloid.2**. The TEM micrographs, Figure 4.14, show irregularly shaped nanoparticles with a mean diameter *ca.* 6 nm. WAXS analysis revealed fcc structure of bulk palladium with a coherence length of at least 4 nm, which is smaller than the mean diameter determined by TEM. This can be attributed to the nanoparticles' lack of crystallinity. TEM observations indicate that the nanoparticles are irregularly shaped that can be attributed to a coalescence of the nanoparticles that is a lack of stabilising effect.

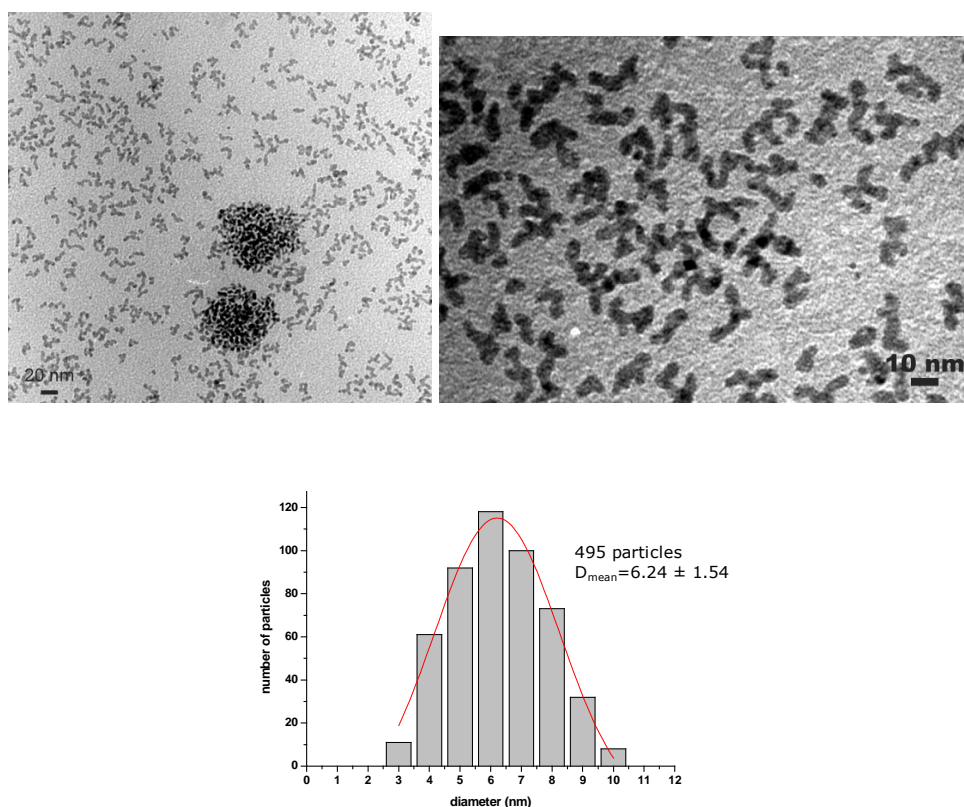


Figure 4.14. Transmission electron micrographs of **Coll.3** and size histogram built from *ca.* 500 nanoparticles

Palladium nanoparticles stabilised with phosphine-phosphite ligand **4**, **Colloid.4**, which has the same carbohydrate backbone than the diphosphite ligand **1**, were synthesised by following the general procedure. The elemental analysis of the black

isolated nanoparticles of **Colloid.4** was 71.59%Pd, 1.97%P, 15.94%C, 1.28%H, which displays a Pd/P ratio of 11/1, much higher than the observed in the colloids **Coll.2** and **Coll.3**.

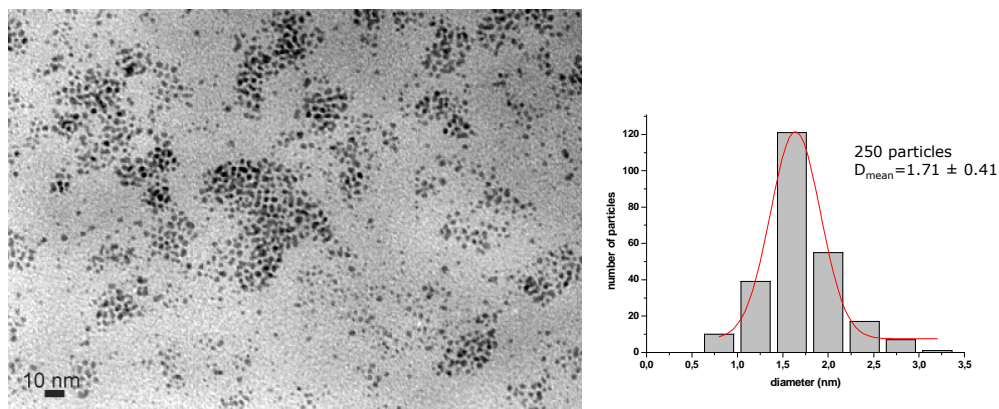


Figure 4.15. Transmission electron micrographs of **Colloid.4** and size histogram built from ca. 250 nanoparticles

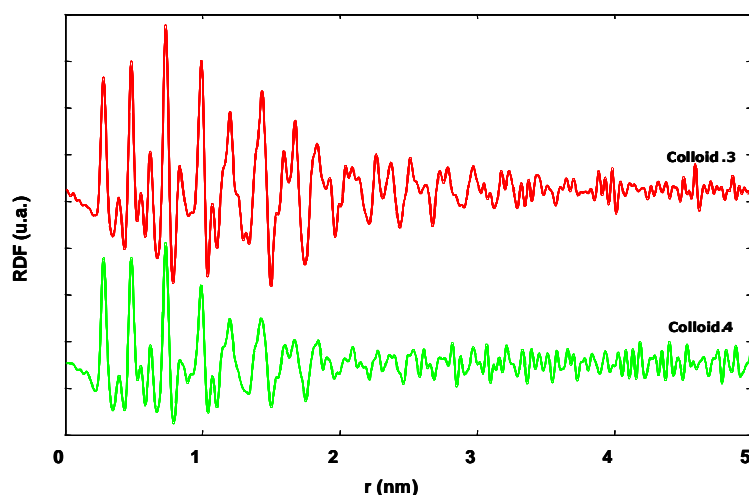


Figure 4.16. RDF of **Colloid.3** and **Colloid.4** obtained from WAXS analysis

The use of phosphine-phosphite ligand **4** to stabilise palladium nanoparticles, **Colloid.4**, led to the formation of different nanoparticles from those obtained with diphosphite ligands. Thus, the TEM analysis revealed well-dispersed, small,

spherical nanoparticles with a mean diameter, *ca.* 2 nm (Figure 4.15), in contrast to the irregularly shaped palladium nanoparticles stabilised with diphosphite ligands **1** to **3** with a mean diameter of *ca.* 4 nm. The spherical shape may indicate better stabilisation and in addition, the size histogram is very narrow. The WAXS analysis revealed fcc structure of the bulk palladium with a coherence length of *ca.* 2.5-3 nm, which means that the nanoparticles were smaller.

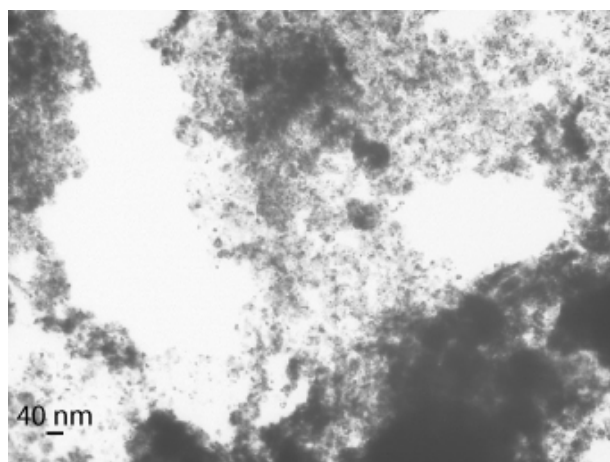


Figure 4.17. Transmission electron micrograph of **Colloid.5**

In order to improve the palladium nanoparticles synthesised with ligand **4**, **Colloid.4**, we synthesised new nanoparticles modifying the following reaction conditions: a) at 60°C, **Colloid.5**, and b) increasing the palladium/ligand ratio to 1/0.4, **Colloid.6**. **Colloid.5** was analysed by TEM, WAXS analysis and elemental analysis, but **Colloid.6** was only analysed by TEM because the nanoparticles did not precipitate. The elemental analysis of the black isolated nanoparticles of **Colloid.5** was 60.67 %Pd, 3.55%P; which displays a Pd/P ratio of 5/1. In both cases the TEM micrographs (Figure 4.17 and 4.19) revealed more agglomerated nanoparticles than when *standard* conditions (room temperature, palladium/ligand ratio 1/0.2) were used, and no isolated nanoparticles were observed.

The WAXS analysis of **Colloid.5** revealed the fcc structure of the bulk palladium with a coherence length of *ca.* 3.5-4 nm. However, the nanoparticles were not

crystallised so well, since the RDF is not well-defined, as for **Colloid.4**, (see Figure 4.18). The TEM analysis showed much more agglomeration than in the case of palladium nanoparticles **Colloid.4**.

We can conclude that palladium nanoparticles stabilised with phosphorus chiral ligands have been successfully synthesised. These colloids are composed of small nanoparticles which display the fcc structure of bulk palladium with a mean diameter of 2-6 nm. TEM analysis of palladium nanoparticles stabilised with diphosphite **1** to **3** revealed small, irregularly-shaped sometimes agglomerated particles with a mean size of *ca.* 4 nm for colloids **Coll.1** and **Coll.2**, and *ca.* 6 nm for colloid **Coll.3**. Ligand **4**, with a phosphine function, made it possible to obtain smaller palladium nanoparticles. **Colloid.4** presents particles with a mean diameter of *ca.* 2 nm, with more regular shape than when diphosphite ligands were used as stabilisers. The palladium nanoparticles **Coll.4** showed more presence of ligand (Pd/P ratio of 11/1 instead of the ratio showed by diphosphite stabilised palladium nanoparticles, 57/1 for **Coll.2** and 60/1 for **Coll.3**, see above) indicating that the ligand interact stronger with the surface than diphosphite ligands.

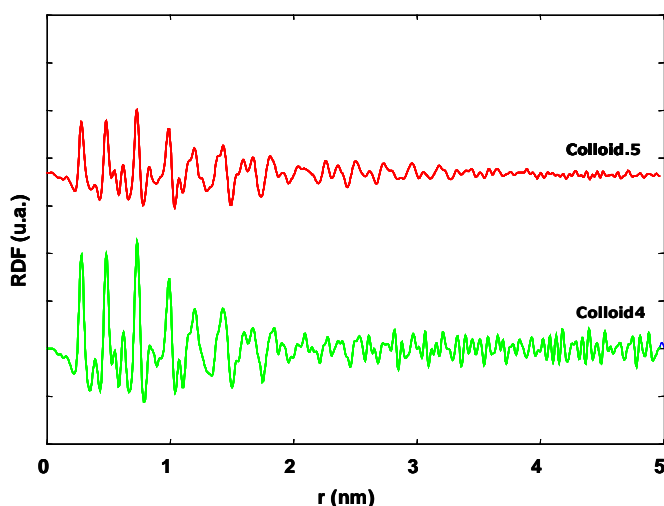


Figure 4.18. RDF of **Coll.4** and **Coll.5** obtained from WAXS analysis

We also studied the effect of the temperature and the palladium/ligand ratio on the nanoparticles stabilised with phosphine-phosphite ligand **4**. We observed that an

increase in the temperature or an increase in the quantity of ligand did not improve the results and led to more agglomeration and no well crystallisation.

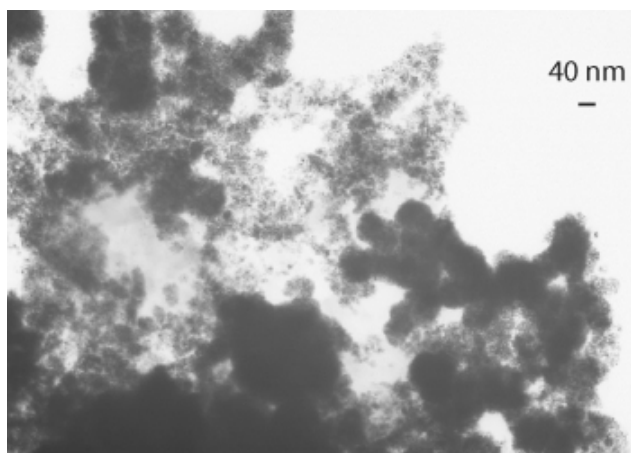
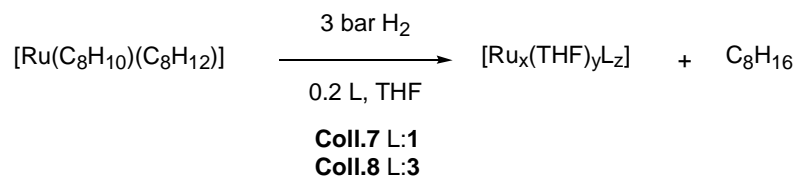


Figure 4.19. Transmission electron micrograph of **Coll.6**

4.2.2 Synthesis of ruthenium nanoparticles from the precursor $[\text{Ru}(\text{C}_8\text{H}_{10})(\text{C}_8\text{H}_{12})]$

Ruthenium nanoparticles were synthesised by the organometallic approach using $[\text{Ru}(\text{C}_8\text{H}_{10})(\text{C}_8\text{H}_{12})]$ ^[126] as metal precursor in the presence of diphosphite ligands **1** and **3**, colloids **Coll.7** and **Coll.8**, respectively, with a Ru/L ratio of 1/0.2.



Scheme 4.8. Synthesis of ruthenium nanoparticles from $[\text{Ru}(\text{C}_8\text{H}_{10})(\text{C}_8\text{H}_{12})]$ in the presence of chiral ligands **1** and **3**

The initial solution of the ruthenium precursor and the ligand in THF was yellow. After pressurization at room temperature under 3 bars of hydrogen, the solution became black in a few minutes. The nanoparticles were isolated by precipitation

with pentane and analysed by TEM, WAXS and elemental analysis. The samples for microscopy analysis were prepared from a drop of the colloidal solution, which was deposited under argon on a holey carbon covered copper grid. The samples for WAXS analysis were prepared from the isolated nanoparticles, which were sealed in 1mm Lindemann glass capillaries.

In both cases the TEM analysis revealed small nanoparticles which were well dispersed on the grid with a mean diameter *ca.* 2.5 nm. However, the shape of the nanoparticles depends on the ligand used. **Colloid.7**, stabilised with diphosphite **1**, showed ruthenium nanoparticles of irregular shape (Figure 4.20), which were agglomerated in some cases. The ruthenium nanoparticles stabilised with diphosphite **3**, **Colloid.8**, appeared in TEM micrographs as spherical nanoparticles without agglomeration (Figure 4.21).

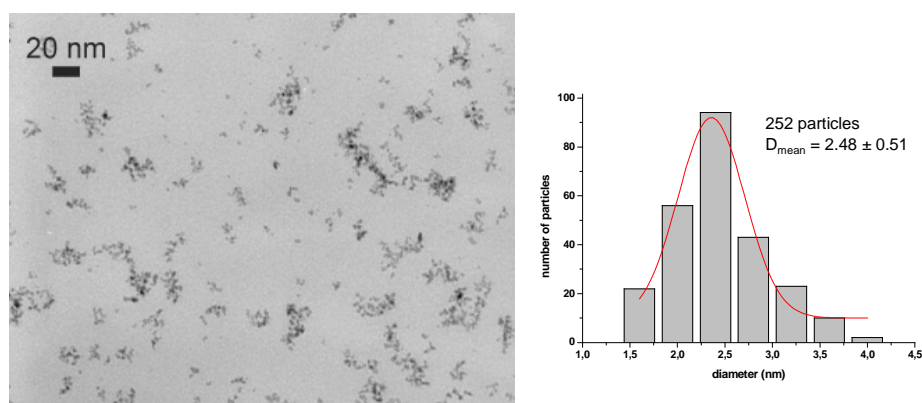


Figure 4.20. Transmission electron micrograph of **Coll.7** and size histogram built from *ca.* 250 nanoparticles

The elemental analysis of the black isolated nanoparticles of **Colloid.7** was 42.19%Ru, 1.86%P, 7.72%C, 1.18%H, which displays a Ru/P ratio of 7/1. The elemental analysis of the black isolated nanoparticles of **Colloid.8** was 44.67%Ru, 1.34%P, 2.40%Si, 24.82%C, 2.99%H, which displays a Ru/P ratio of 10/1. Although **Colloid.7** and **Colloid.8** had similar percentages of ruthenium and phosphorus in the elemental analysis and similar Ru/P ratios, which indicated similar amounts of ligand in both colloids, the amount of carbon and hydrogen is

greater for **Colloid.8**. This suggests the presence of more solvent on the surface of the nanoparticles for **Colloid.8** than for **Colloid.7**.

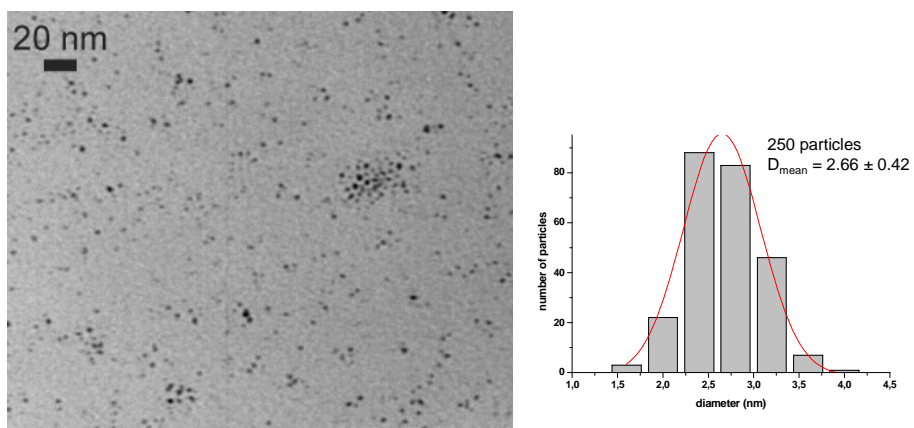


Figure 4.21. Transmission electron micrograph of **Colloid.8** and size histogram built from *ca.* 250 nanoparticles

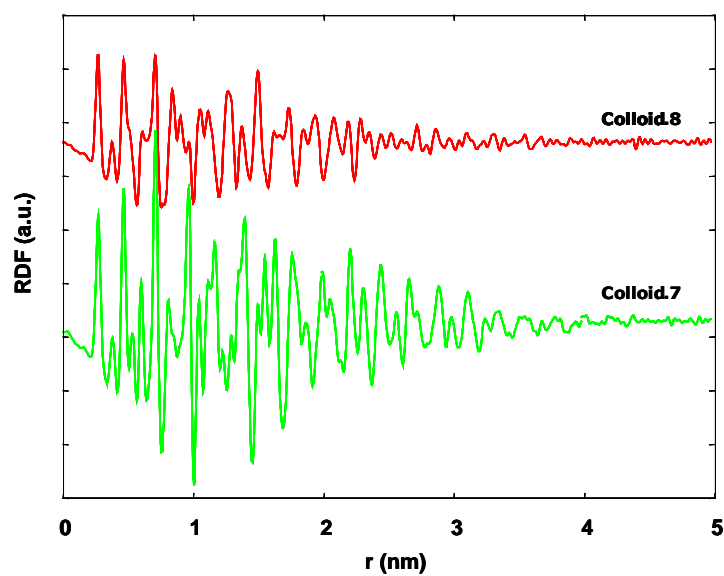


Figure 4.22. RDF of **Colloid.7** and **Colloid.8** obtained from WAXS analysis

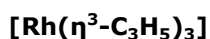
WAXS analysis of **Colloid.7** (Figure 4.22) showed the peaks corresponding to well-crystallised hcp (hexagonal close-packed) ruthenium particles with a coherence length of *ca.* 3 nm, which is in good accordance with the mean diameter determined by TEM analysis. On the other hand, the WAXS analysis of **Colloid.8**, which would be expected to be similar to that of **Colloid.7**, revealed a different RDF, perhaps suggesting that the stabiliser behaves differently. We can conclude that ruthenium nanoparticles stabilised with ligand **1**, **Colloid.7**, are well-crystallised nanoparticles, while for **Colloid.8**, the ruthenium nanoparticles stabilised with ligand **3**, displayed a RDF that indicated that the nanoparticles were not well-crystallised. Further work with **Colloid.8** is required to better understand these differences between the ligand behaviours.

4.2.3 Synthesis of rhodium nanoparticles

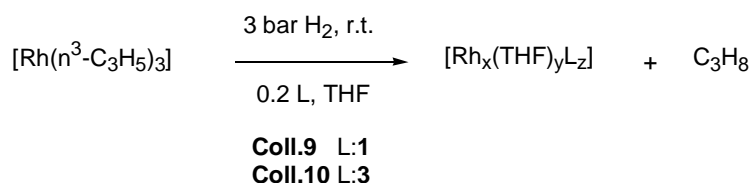
Rhodium nanoparticles were obtained by decomposition of two different rhodium precursors, $[\text{Rh}(\eta^3\text{-C}_3\text{H}_5)_3]$ ^[127, 128] and $[\text{Rh}(\mu\text{-OMe})(\text{COD})_2]$ ^[129] which were synthesised by previously described methods. The nanoparticles were synthesised in tetrahydrofuran solution in the presence of various stabilisers, at room temperature and under 3 bars of hydrogen. Two different precursors and various stabilisers were used to compare the effect of these variables on the nanoparticles obtained.

The rhodium complex $[\text{Rh}(\eta^3\text{-C}_3\text{H}_5)_3]$ has been successfully used before as the metal precursor in the synthesis of rhodium nanoparticles.^[69, 70] Small, mean diameter of 5 nm, and well dispersed rhodium nanoparticles were synthesised from this precursor in the presence of HDA (hexadecylamine), but when the surfactant HEA-16-Cl (N,N-dimethyl-N-cetyl-N-(2-hydroxyethyl) ammonium chloride)^[41, 95] was used as stabiliser sponge-like agglomerates with 34 nm of mean diameter were obtained.^[69] Recently, rhodium nanoparticles were synthesised from this precursor by an original method, namely the solid-state decomposition under dihydrogen of an organometallic precursor dispersed in polymer films or directly as nanocrystals.^[70] The decomposition of $[\text{Rh}(\eta^3\text{-C}_3\text{H}_5)_3]$ in a standard PMMA film (poly(methylmethacrylate)) led to small nanoparticles of about 2 nm of diameter.

4.2.3.1 Synthesis of rhodium nanoparticles from the precursor



Rhodium nanoparticles have been synthesised from the precursor $[\text{Rh}(\eta^3\text{-C}_3\text{H}_5)_3]$, in the presence of diphosphite ligands **1** or **3** as stabilisers, following the reaction presented in Scheme 4.9.



Scheme 4.9. Synthesis of rhodium nanoparticles from $[\text{Rh}(\eta^3\text{-C}_3\text{H}_5)_3]$ in the presence of chiral ligands **1** and **3**

The initial solution of the rhodium precursor in the presence of diphosphite ligand, **1** or **3**, was pale yellow, and became black in a few minutes, which confirmed the decomposition of the rhodium precursor. After 18 hours of vigorous stirring under 3 bars of hydrogen, the evaporation of the solvent gave a black precipitate which was washed several times with pentane to afford **Colloid.9** and **Colloid.10**, respectively. The nanoparticles synthesised were analysed by TEM, WAXS and elemental analysis.

The elemental analysis of the black isolated nanoparticles of **Colloid.9** was 34.23%Rh, 0.61%P, 4.70%C, 0.47%H, which displays a Rh/P ratio of 17/1. The elemental analysis of the black isolated nanoparticles of **Colloid.10** was 37.74%Rh, 2.48%P, 3.88 %Si, 6.79%C, 0.59%H, which displays a Rh/P ratio of 5/1.

Figures 4.23 and 4.24 present the transmission electron micrographs of **Colloid.9** and **Colloid.10**, respectively obtained from $[\text{Rh}(\eta^3\text{-C}_3\text{H}_5)_3]$ and diphosphite ligands **1** and **3**. In both cases the TEM micrographs revealed similar nanoparticles which were well dispersed, small and with a spherical shape. Small agglomerates consisting of a few nanoparticles were observed. Size histograms were built of at

least 150-250 particles and mean diameters of *ca.* 3 nm and *ca.* 2 nm were found for **Colloid.9** and **Colloid.10**, respectively.

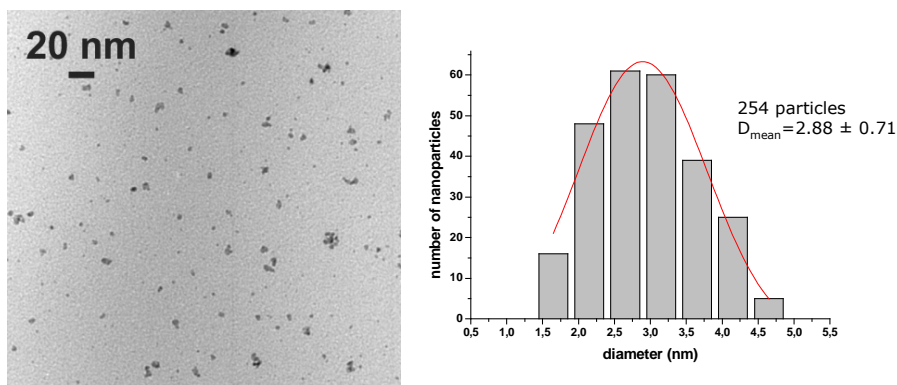


Figure 4.23. Transmission electron micrograph of **Coll.9** and size histogram built from *ca.* 250 nanoparticles

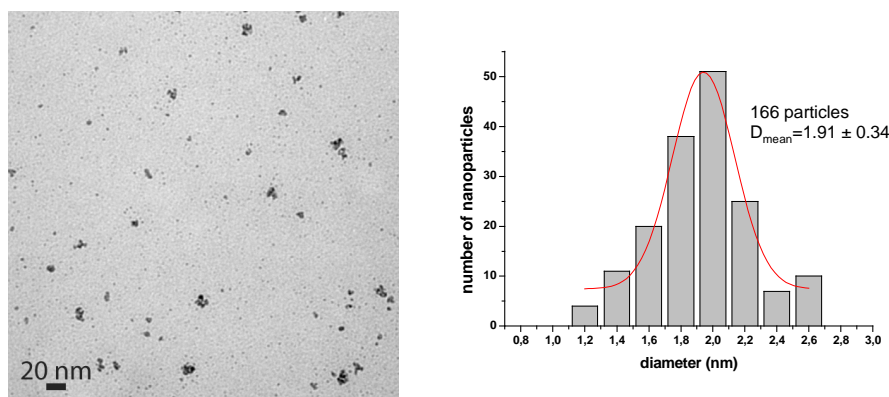


Figure 4.24. Transmission electron micrograph of **Coll.10** and size histogram built from *ca.* 170 nanoparticles

In **Colloid.9** and in **Colloid.10**, the WAXS measurement (Figure 4.25) revealed, identical well-crystallised rhodium nanoparticles displaying a fcc structure and a coherence length near 3.5-4 nm. However, **Colloid.9** showed particles with a slightly shorter coherence length than **Colloid.10**, which is in agreement with the size determined by TEM micrographs. Nevertheless, in both cases the coherence length determined by WAXS measurement was higher than the mean diameter

resulting from TEM observations. This phenomena is unusual and probably comes from the fact that larger particles can strongly influence the measurement even if they are not very numerous. The difference between the mean diameter determined by TEM and the coherence length is higher for **Colloid.10**.

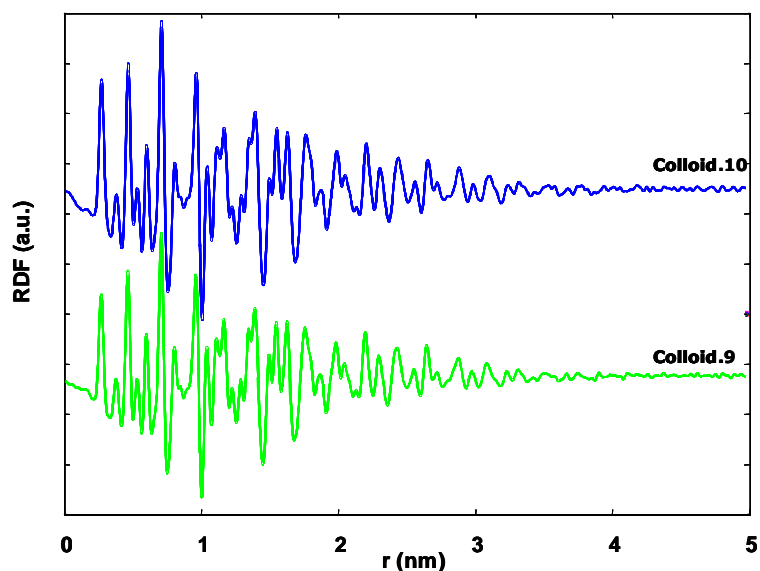


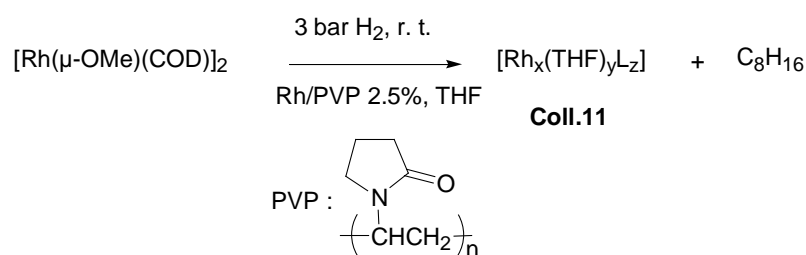
Figure 4.25. RDF of **Coll.9** and **Coll.10** obtained from WAXS analysis

4.2.3.2 Synthesis of rhodium nanoparticles from the precursor $[\text{Rh}(\mu\text{-OMe})(\text{COD})]_2$

To our knowledge the $[\text{Rh}(\mu\text{-OMe})(\text{COD})]_2$ complex had not been previously used as a metal precursor to synthesise rhodium nanoparticles. The advantage of this precursor is that is easier to prepare than $[\text{Rh}(\eta^3\text{-C}_3\text{H}_5)_3]$ and other rhodium complexes. However, methanol is produced during the decomposition. So, first of all, we tested the decomposition of this precursor in the presence of a *classical* stabiliser like PVP (polyvinylpyrrolidone MW= 40000), a well-known organic polymer in the nanoparticles domain.

Rhodium nanoparticles were synthesised from the precursor $[\text{Rh}(\mu\text{-OMe})(\text{COD})]_2$ in the presence of PVP, namely **Colloid.11**, according to the synthesis presented in Scheme 4.10.

The initial THF solution of the rhodium precursor and PVP (Rh/PVP 2.5%) was pale yellow and became brown-black under 3 bar of hydrogen pressure due to the decomposition of the precursor. After one hour, the solution was completely black. We maintained the vigorous magnetic stirring for 18 hours. The evaporation of the solvent gave a grey precipitate which was washed several times with pentane. The nanoparticles synthesised were analysed by TEM, WAXS and elemental analysis.



Scheme 4.10. Synthesis of rhodium nanoparticles from $[\text{Rh}(\mu\text{-OMe})(\text{COD})]_2$ in the presence of PVP

The elemental analysis of the grey isolated nanoparticles of **Colloid.11** was 9.31%Rh, 53.71%C, 7.46%H, 9.95%N. The TEM micrograph of **Colloid.11** (Figure 4.26) shows well dispersed, small nanoparticles.

The TEM micrograph of **Colloid.11** at higher magnification (Figure 4.26) showed small aggregates of a few nanoparticles with an irregular shape with a mean diameter of *ca.* 3 nm. This agrees with the WAXS measurement (Figure 4.27) that revealed well-crystallised rhodium nanoparticles displaying a fcc structure and a coherence length of 3.5 nm.

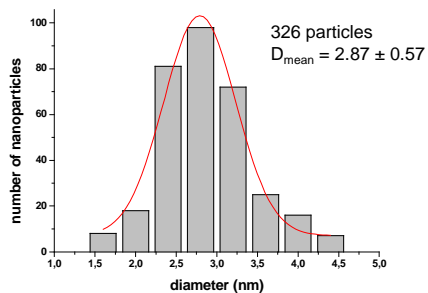
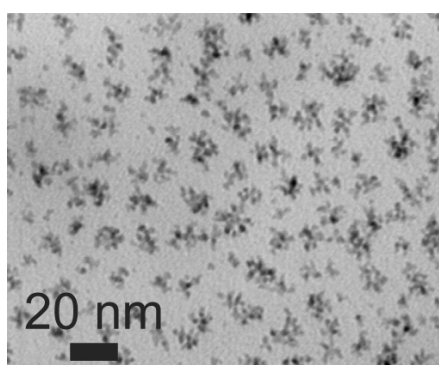
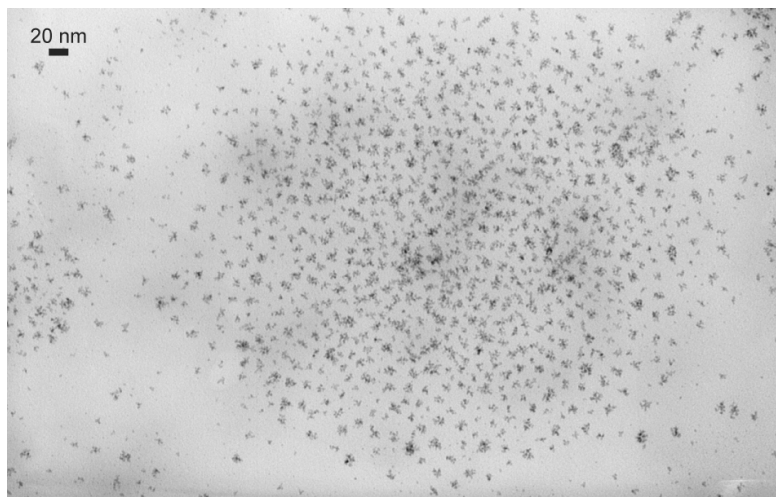


Figure 4.26. Transmission electron micrographs of **Coll.11** and size histogram built from ca. 325 nanoparticles

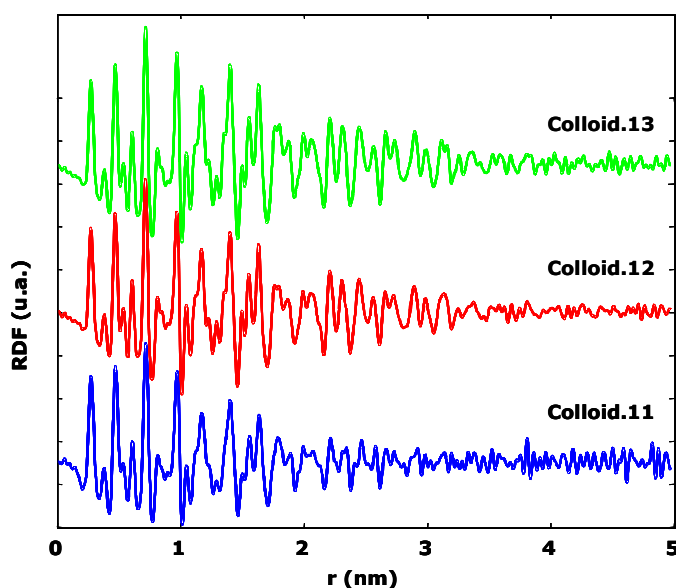
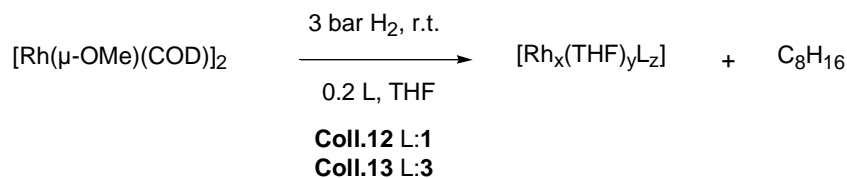


Figure 4.27. RDF of **Colloid.11**, **Colloid.12** and **Colloid.13** obtained from WAXS analysis

Rhodium nanoparticles from the precursor $[\text{Rh}(\mu\text{-OMe})(\text{COD})]_2$ were also synthesised using diphosphite chiral ligands **1** and **3** (Scheme 4.11) as stabilisers. The decomposition takes place in a similar way to when PVP was used as stabiliser (Scheme 4.10). The rhodium nanoparticles stabilised with diphosphite ligand **1**, **Colloid.12**, and with diphosphite ligand **3**, **Colloid.13**, were analysed by TEM, WAXS and elemental analysis.



Scheme 4.11. Synthesis of rhodium nanoparticles from $[\text{Rh}(\mu\text{-OMe})(\text{COD})]_2$ in the presence of chiral ligands **1** and **3**

The elemental analysis of the black isolated nanoparticles of **Colloid.12** was 73.69%Rh, 0.10%P, 2.84%C, 0.10%H, which displays a Rh/P ratio of 222/1. The

elemental analysis of the black isolated nanoparticles of **Colloid.13** was 16.71%Rh, 0.11%P, 5.24%Si, 4.59%C, 0.11%H, which displays a Rh/P ratio of 45/1.

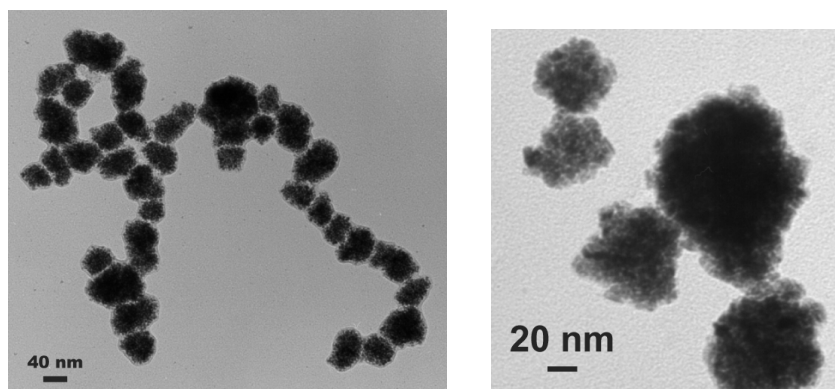


Figure 4.28. Transmission electron micrographs of **Coll.12**

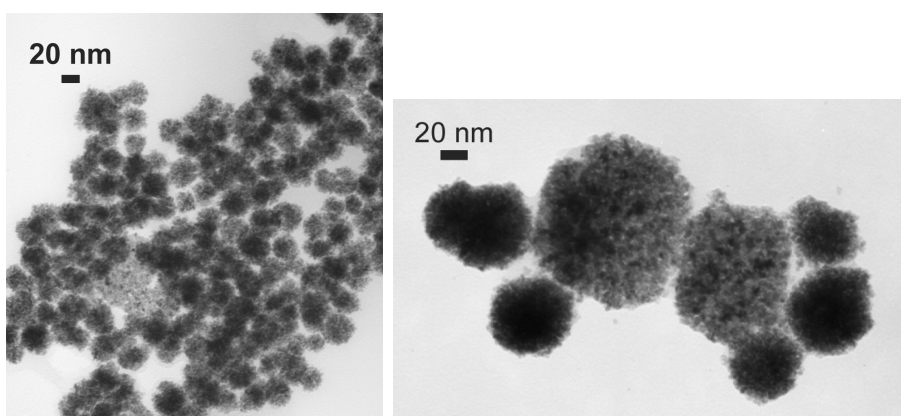


Figure 4.29. Transmission electron micrographs of **Coll.13**

TEM micrographs of **Colloid.12** and **Colloid.13** (Figure 4.28 and 4.29, respectively) showed similar large, sponge-like spherical superstructures which in some cases were aggregated among them. For **Colloid.12** these superstructures have a mean diameter of *ca.* 50 nm and for **Colloid.13** of *ca.* 35 nm. At highest magnification we observed that these large structures in fact seem to be composed of small individual nanoparticles with a diameter of about 4 nm in both colloids. The WAXS measurement (Figure 4.27) revealed that in both colloids, **Colloid.12** and **Colloid.13**, had identical, well-crystallised, rhodium nanoparticles displaying a fcc

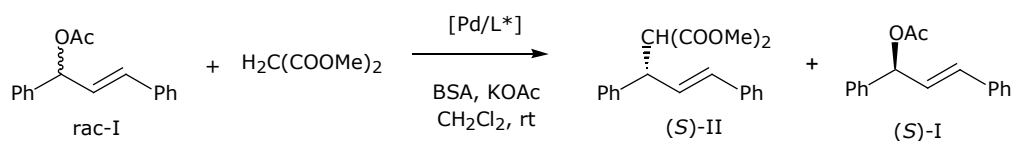
structure and a coherence length of 4 nm. Although the TEM and WAXS analysis indicate that these superstructures are agglomerates of small nanoparticles, we can not exclude the possibility that they are large, porous and polycrystalline particles. However, further analysis are necessary to distinguish between these two possibilities.

Similar sponge-like structures have been previously described with rhodium nanoparticles^[69, 130] and with such metal nanoparticles as ruthenium^[66, 76], nickel^[64] and platinum^[131-133]. These studies have observed that the reaction parameters (metal precursor, method of synthesis, temperature, solvent, etc.) played an important role in the final properties of the nanoparticles (size, shape, etc.). We also observed that when PVP is used as stabiliser, nanoparticles were small but changing of the PVP for diphosphite ligands led to the formation of large structures. This may mean that the diphosphite ligands have a lower stabilising effect than the PVP. On the other hand, we have observed that if another rhodium precursor, $[\text{Rh}(\eta^3\text{-C}_3\text{H}_5)_3]$ is used, in the same reaction conditions with the same diphosphite ligands **1** and **3** as stabilisers, the resulting nanoparticles are small (see Figures 4.23 and 4.24). The characteristics of the nanoparticles synthesised depend on the rhodium precursor used and can be attributed to the products obtained by the decomposition of the precursor. The decomposition of the olefinic precursor $[\text{Rh}(\eta^3\text{-C}_3\text{H}_5)_3]$ leads to the production of propane which cannot produce strong bonds with the growing metal surface in these conditions.^[17] This is not the case with the rhodium precursor $[\text{Rh}(\mu\text{-OMe})(\text{COD})]_2$. Indeed the decomposition of this precursor produces cyclooctane and methanol which remain in the solution. Methanol can interact with the surface atoms of the nanoparticles. Previous studies demonstrated that the concentration of different alcohols in the reaction media affects the characteristics of the nanoparticles synthesised.^[66, 69, 76] In our case, the presence of methanol can enhance the solubility of the PVP leading to better stabilised nanoparticles (small and well dispersed, see Figure 4.26) than diphosphite ligands. However, when diphosphite ligands are used as stabilisers the presence of cyclooctane and methanol can lead to the formation of droplets segregated of the rest of the solvent in which agglomerates may be form. This behaviour was observed in the synthesis of ruthenium nanoparticles from $[\text{Ru}(\text{C}_8\text{H}_{10})(\text{C}_8\text{H}_{12})]$ in the presence of alcohols.^[16, 76]

4.2.4 Application in catalysis of metal nanoparticles

Allylic alkylation

In the frame of a collaboration with the Universitat de Barcelona and Laboratoire de Chimie de Coordination CNRS (Toulouse) we have studied the application of palladium nanoparticles stabilised with diphosphite ligands **2** and **3**, **Coll.2** and **Coll.3**, respectively, in palladium-catalysed allylic alkylation of *rac*-3-acetoxy-1,3-diphenyl-1-propene with dimethyl malonate (Scheme 4.12).

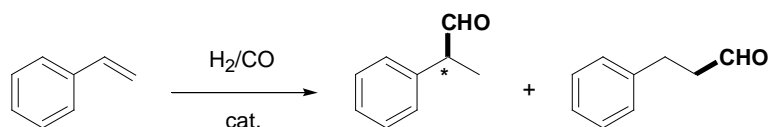


Scheme 4.12. Asymmetric allylic alkylation of *rac*-3-acetoxy-1,3-diphenyl-1-propene with dimethyl malonate

The aim is to compare the influence of configuration of the stereocenter at position 3 (**2**), the presence of phosphine-phosphite moieties (**4**) instead of diphosphite, and the existence of C_2 -symmetry ligands (**3**), with colloids stabilised by ligand **1**, **Coll.1**. The application of **Colloid.1** system in this reaction lead to an enantiomeric excess of >95%(*S*) in II with high kinetic resolution in the substrate (*rac*-I) (89% (*S*) in the remaining substrate) at 56% of conversion.^[79] **Colloid.2** system was not stable under catalytic conditions showing not reproducible results. **Colloid.3** system led also to an enantiomeric excess of >98%(*S*) in II with high kinetic resolution in the substrate (*rac*-I) (98% (*S*) in the remaining substrate). This behaviour is similar to that of **Colloid.1**, although in this case the system slowly evolves until a 73% of conversion, while for **Colloid.1** the reaction stops at 56% of conversion and does not evolve even after 7 days of reaction. This result proves that the excellent kinetic resolution in the reaction of allylic alkylation is not an singular case for **Colloid.1**, but a more general behaviour of palladium-diphosphite nanoparticles.

Hydroformylation of styrene

Colloid.12 and **Colloid.13**, which contain rhodium nanoparticles synthesised from the precursor $[\text{Rh}(\mu\text{-OMe})(\text{COD})]_2$ in the presence diphosphite ligands **1** and **3**, respectively, have been used as catalyst in the rhodium-catalysed asymmetric hydroformylation of styrene (Scheme 4.13). The results are given in Tables 4.1 and 4.2. We used these colloids in order to optimise the conditions of this reaction and then apply them to other rhodium colloids.



Scheme 4.13. Hydroformylation reaction

Table 4.1. Styrene hydroformylation with **Colloid.12** and **Colloid.13**^a

Entry	Catalyst	Rh/L/S ^b	t(h)	% conv. ^c	% ald. ^d	% regio. ^e	% ee
1	Coll.12	1/-/200	24	28	92	57	0
2	Coll.12	1/0.2/200	24	11	97	>99	40 (S)
3	Coll.13	1/-/200	24	95	97	54	13 (S)
4	Coll.13	1/0.2/200	24	80	97	90	24 (S)

^a3 mg. nanoparticle, temp.: 80°C, P=20 bar P_{co}/H₂=1, Rh/S 1:200 styrene 5.8 mmol, 10 ml. toluene ^bMolar ratio between rhodium, excess ligand added to the catalysis and substrate ^c% conversion styrene G.C. ^d% 2-phenylpropanal + 3-phenylpropanal ^e% 2-phenylpropanal

The reaction was carried out at 80°C and 20 bar of pressure (P_{co}/H₂=1) with and without the addition of an excess of the respective ligand in the catalytic media. For the **Colloid.12** catalytic system, conversions were in both cases (Table 4.1, entry 1 and 2). The **Colloid.13** catalytic system was more active in the same conditions (Table 4.1, entry 3 and 4). In all cases we observed a high selectivity to the aldehydes (upper 90%). The addition of the respective free ligand to the catalysis led to a less active but more regioselective catalyst system. The enantioselectivity of the catalytic system was also affected by the addition of ligand. For **Colloid.12** the addition of free ligand **1** increased the enantioselectivity from 0% to 40% (S)

(Table 4.1, entries 1 and 2) and for **Colloid.13** the addition of the free ligand **3** increased the enantioselectivity from 13% to 24% (*S*) (Table 4.1, entries 3 and 4).

The comparison of TEM micrographs before and after catalysis (Figure 4.30 and 4.31) did not show any significant change in the size and shape of the particles, indicating that they were stable under the catalytic reaction conditions.

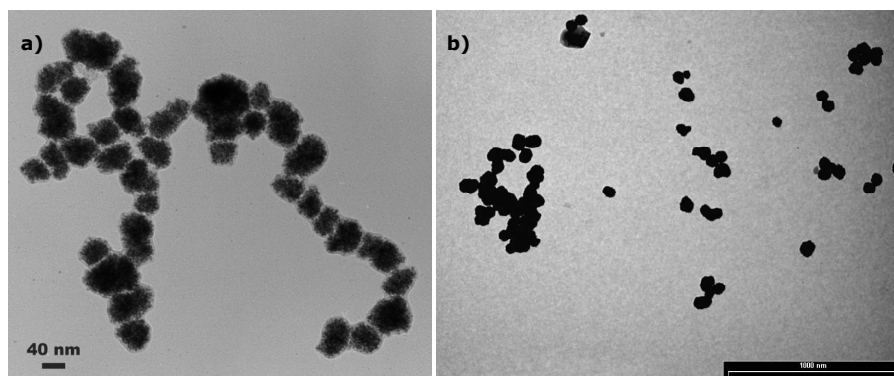


Figure 4.30. Transmission electron micrographs of **Colloid.12** a) before and b) after catalysis

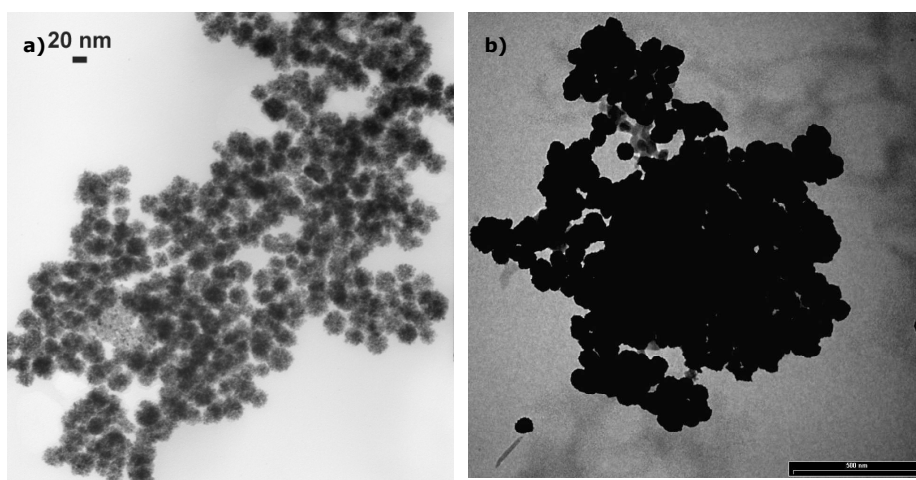


Figure 4.31. Transmission electron micrograph of **Colloid.13** a) before and b) after catalysis

In an attempt to obtain more information about colloidal catalysis, the colloids were compared to molecular equivalent systems. Table 4.2 gives the results obtained

with the colloidal systems, **Colloid.12** and **Colloid.13**, and with the respective molecular systems, **Molecular.12** and **Molecular.13**. In both cases, we studied the effect of the substrate concentration on the colloidal systems. In addition, the effect of the excess of ligand has been studied for **Colloid.13** catalytic system.

Table 4.2. Styrene hydroformylation with **Colloid.12** and **Colloid.13**^a

Entry	Catalyst	Rh/L/S ^b	t (h)	% conv. ^c	TOF (h ⁻¹)	% ald. ^d	% regio. ^e	% ee
1	Mol.12 ^f	1/1/200	15	92	-	98	95	36 (S)
2	Coll.12	1/0.2/200	15	3	0.7	41	>99	-
3			30	10	0.9	98	>99	-
4			45	35	2.2	98	95	45 (S)
5			15	2	0.8	71	>99	-
6	Coll.12	1/0.2/400	30	8	1.4	97	>99	-
7			45	33	3.9	98	97	47 (S)
8			15	2	0.4	90	>99	-
9	Coll.12	1/0.1/200	30	11	0.9	98	>99	-
10			45	37	2.3	98	96	43 (S)
11			Mol.13 ^g	1/1/200	15	99	-	>99
12	Coll.13	1/0.2/200	15	31	24.5	92	97	-
13			30	70	27.5	98	95	-
14			45	90	23.9	98	95	31 (S)
15	Coll.13	1/0.2/400	15	35	55.1	93	97	-
16			30	76	60.4	99	95	-
17			45	94	50.3	99	95	32 (S)

^a3 mg. nanoparticle, temp.: 70°C, P=40 bar Pco/H₂=1, Rh/S 1:200 styrene 5.8 mmol, 10 ml. toluene
^bMolar ratio between rhodium, excess ligand added to the catalysis and substrate ^c% conversion styrene
^dG.C. ^e% 2-phenylpropanal + 3-phenylpropanal ^f% 2-phenylpropanal [Rh]= 9.04x10⁻⁴M temp.: 70°C, P=40
bar Pco/H₂=1, Rh/S 1:200 styrene 1.8 mmol, 10 ml. toluene ^g Substrate/Rh=200, styrene 2.7 mmol,
[Rh(acac)(CO)₂] 0.0135mmol temp: 60°C P=20 bar, 15 ml toluene Pco/H₂=1

If we compare the results of the molecular systems with the ones of the colloidal systems we can observe that the molecular system is highly active, with total conversion at 15 hours of reaction (Table 4.2, entries 1 and 11). The colloidal

systems, **Colloid.12** and **Colloid.13**, on the other hand, are not very active: the TOF's of **Colloid.12** were less than 4 h^{-1} , while for **Colloid.13** they were around 50 h^{-1} . Although the regioselectivity with the molecular and the colloidal systems is similar, the enantioselectivity is higher with the colloidal systems than with the molecular ones.

The addition of a high quantity of substrate led to more active catalysts in both cases, **Colloid.12** and **Colloid.13**, (Table 4.2, entries 5-7 and 15-17) which indicated that the rate is proportional to the concentration of the substrate. An increase in the free ligand added (Table 4.2, entries 2 to 4 vs. 8 to 10) does not affect the activity and the selectivity.

In order to better compare between the colloidal and molecular catalytic systems, which display very different reaction rates, a series of experiments was carried out. The catalyst concentration of the homogenous molecular system was decreased, so that the reaction rates were comparable to those of the colloidal ones. The results are summarised in Table 4.3.

Table 4.3. Styrene hydroformylation with diluted **Molecular.12** catalyst^a

Entry	Rh/L/S ^b	t (h)	% conv. ^c	TOF (h ⁻¹)	% ald. ^d	% regiosec. ^e	% ee
1	1/1/200 ^f	15	92	12.2	98	95	36(S)
2	1/1/2000 ^g	15	84	111.9	96	87	0
3	1/1/20000 ^h	15	35	466.7	99	84	-
4		30	91	608.0	97	79	0
5	1/1/100000 ⁱ	15	7	433.3	>99	>99	-
6		30	59	1963.3	93	85	0
8	1/1/200000 ^j	15	0	-	-	-	-
9		30	<1	-	>99	>99	-

^atemp.: 70°C, P=40 bar P_{co}/H₂=1, styrene 1.8 mmol, 10 ml. toluene ^bMolar ratio between rhodium, excess ligand added in the catalysis and substrate ^c% conversion styrene G.C. ^d%2-phenylpropanal + 3-phenylpropanal ^e% 2-phenylpropanal ^f[Rh]= $9.04 \times 10^{-4} \text{M}$, ^g[Rh]= $9.04 \times 10^{-5} \text{M}$, ^h[Rh]= $9.04 \times 10^{-6} \text{M}$, ⁱ[Rh]= $1.81 \times 10^{-6} \text{M}$, ^j[Rh]= $9.04 \times 10^{-7} \text{M}$

Table 4.4. Styrene hydroformylation with diluted **Molecular.12** catalyst and excess of ligand **1**^a

Entry	Rh/L/S ^b	t (h)	% conv. ^b	TOF (h ⁻¹)	% ald.	% regiosec. ^c	% ee
1	1/1/200	15	89	11.9	96	96	37(S)
2	1/1/2000	15	35	46.7	94	91	-
3		30	86	57.1	94.1	95	36 (S)
4	1/1/20000	15	5	60.0	80	>99	-
5		30	16	109.3	90	>99	-
6		45	85	373.3	94	92	19 (S)
7	1/1/100000	15	1	-	-	>99	-
8		30	7	236.7	82	>99	-
9		45	15	342.2	87	>99	-
10		60	30	506.7	89	>99	29 (S)
10	1/1/200000	15	<1	-	-	>99	-
11		30	8	513.3	84	>99	-
12		45	18	795.6	88	>99	-
13		60	31	1013.3	89	>99	29 (S)

^atemp.: 70°C, P=40 bar P_{co}/H₂=1, styrene 1.8 mmol, ligand **1** 5.8 mmol, 10 ml. toluene ^bMolar ratio between rhodium, excess ligand added to the catalysis and substrate ^c% conversion styrene G.C.^d %2-phenylpropanal + 3-phenylpropanal ^e% 2-phenylpropanal ^f[Rh]= 9.04x10⁻⁴M, ^g[Rh]= 9.04x10⁻⁵M, ^h[Rh]= 9.04x10⁻⁶M, ⁱ[Rh]= 1.81x10⁻⁶M, ^j[Rh]= 9.04x10⁻⁷M

It appears that a decrease in the catalyst concentration decreases the conversion. This is in agreement with the reaction kinetics of the hydroformylation reaction, which is proportional to the rhodium concentration.^[134] With dilutions higher than 1/1/2000 (Table 4.3, entries 2, 4 and 6) no enantioselectivity was observed. This may be due to the formation of [RhH(CO)₄] which is a highly active achiral hydroformylation catalyst.^[134] The formation of this species is favoured for small concentration of rhodium respect to the CO quantity in the medium, which displaces the coordinated ligand. So we decided to make a new series of essays with diluted molecular systems (see Table 4.4), in which we added the same concentration of ligand as in the colloidal systems (Table 4.1 and 4.2). We observed that the presence of added ligand led to lower activity (e. g., Table 4.3, entry 3 and 4 vs. Table 4.4 entries 4 and 5) but catalysts that were more enantioselective. This

indicates that the excess of ligand is enough to maintain the active species with ligand coordinated.

The results of the experiments carried out with the diluted molecular and the colloidal catalytic systems could suggest the formation of molecular system. Nevertheless, while the molecular system, diluted or not, displayed enantioselectivities in the range 19-37% (*S*), the colloidal ones showed enantioselectivities as high as 45% (*S*) (Table 4.2, entries 4, 7 and 10).

Table 4.5. Poison Test.
Styrene hydroformylation with **Colloid.12** and **Molecular.12** catalyst^a

Entry	Catalyst	Rh/L/S/poison ^c	t (h)	% conv ^d	TOF (h ⁻¹)	% ald. ^e	% regio. ^f	% ee
1	Mol.12^b	1/1/200/-	15	92	-	98	95	36 (<i>S</i>)
2	Mol.12^b	1/1/200/4 (CS ₂)	15	96	-	>99	93	15 (<i>S</i>)
3	Mol.12^b	1/1/200/100 (Hg)	15	96	-	>99	92	15 (<i>S</i>)
4	Coll.12	1/0.2/200/-	15	3	0.7	41	>99	-
5			30	10	0.9	98	>99	-
6			45	35	2.2	98	95	45 (<i>S</i>)
7	Coll.12	1/0.2/200/4	15	14	2.6	>99	>99	-
8		(CS ₂)	30	47	4.2	>99	96	40 (<i>S</i>)
9			45	64	3.8	>99	96	36 (<i>S</i>)
10	Coll.12	1/0.2/200/100	15	3	0.5	>99	>99	-
11		(Hg)	30	18	1.6	>99	95	33 (<i>S</i>)
12			45	38	2.3	>99	95	30 (<i>S</i>)

^a3 mg. nanoparticle, temp.: 70°C, P=40 bar P_{co}/H₂=1, Rh/S 1:200 styrene 5.8 mmol, 10 ml. toluene
^b[Rh]= 9.04x10⁻⁴M temp.: 70°C, P=40 bar P_{co}/H₂=1, Rh/S 1:200 styrene 1.8 mmol, 10 ml. toluene
^cMolar ratio between rhodium, excess ligand added to the catalysis, substrate and poison
^d% conversion styrene
^eG.C. %2-phenylpropanal + 3-phenylpropanal
^f% 2-phenylpropanal

However, the fact that the asymmetric induction between **Colloid.12** and **Molecular.12** systems is different suggests that the catalytic system is different. In order to rule out the possibility of a small amount of molecular catalyst to be formed from the particles a series of experiments were carried out in the presence

of *classical* poisons (CS_2 and Hg). The results of these test are summarised in Table 4.5.

The molecular system tested in the presence of CS_2 or Hg (Table 4.5, entries 2 and 3) gave similar results. The activity and regioselectivity of the poisoned and unpoisoned molecular systems are almost identical (Table 4.5, entry 1). However, in the presence of CS_2 or Hg the enantioselectivity decreases from 36% to 15%ee.

In the colloidal system the presence of CS_2 (Table 4.5, entries 7 to 9) led to an increase of the activity but a slightly decrease on the enantioselectivity, than in the colloidal catalyst system without poison. When Hg was used as poison (Table 4.5, entries 10 to 12) the activity of the system was quite similar to that of the system without poison (Table 4.5, entries 4 to 6), but the enantioselectivity was clearly smaller. It is expected that the addition of poison to the active surfaces (colloidal or heterogeneous) led to a decrease in the activity.

Nevertheless, it is also necessary to consider that rhodium does not amalgamate with $\text{Hg}(0)^{[135]}$ and CS_2 begins to dissociate from the heterogeneous catalyst at higher temperatures than 50°C , ^[135] and the experiments were carried out at 70°C , these results are not conclusive. The results obtained with colloidal and molecular catalytic systems, and the poisoning tests suggest the formation of small amounts of molecular system form the colloidal one, however, these are difficult to analyse and further analysis are needed to be able to clearly conclude.

4.3 Conclusions

New palladium, ruthenium and rhodium nanoparticles have been successfully synthesised in the presence of carbohydrate derivative ligands (**1-4**). We observed that the shape, size and dispersion of the nanoparticles depend strongly on the metal precursor and the stabiliser used.

Palladium nanoparticles were synthesised from $[\text{Pd}_2(\text{dba})_3]$ with phosphite ligands **2** and **3** and phosphine-phosphite ligand **4** as stabilisers. The synthesis was done following the organometallic approach, at room temperature and under 3 bars of

hydrogen pressure. In the presence of diphosphite ligands, small nanoparticles (diameter ca. 3.5-4 nm) well-crystallised and contain a few agglomerates were obtained. When phosphine-phosphite ligand **4** was used as stabiliser, smaller nanoparticles could be prepared. This indicates that the nature of the ligand has a strong influence on the morphology of the nanoparticles synthesised. We also studied the effect of the temperature and the palladium/ligand ratio on the nanoparticles stabilised with phosphine-phosphite ligand **4**. We observed that an increase in the temperature or the quantity of ligand did not improve the results and led to more agglomeration and no well crystallisation.

Ruthenium nanoparticles have also been synthesised by the organometallic approach using $[\text{Ru}(\text{C}_8\text{H}_{10})(\text{C}_8\text{H}_{12})]$ as metal precursor and diphosphite ligands **1** and **3** as stabilisers, at room temperature under 3 bars of hydrogen pressure. When diphosphite ligand **1** was used as stabiliser, nanoparticles were well-crystallised with a mean diameter ca. 3 nm. However, when diphosphite ligand **3** was used not well-crystallised nanoparticles were obtained.

Rhodium nanoparticles were obtained by decomposition of two different rhodium precursors, $[\text{Rh}(\eta^3\text{-C}_3\text{H}_5)_3]$ and $[\text{Rh}(\mu\text{-OMe})(\text{COD})]_2$, following the organometallic approach. The rhodium nanoparticles produced from $[\text{Rh}(\eta^3\text{-C}_3\text{H}_5)_3]$ were synthesised in tetrahydrofuran in the presence of diphosphite ligands **1** and **3** as stabilisers at room temperature and under 3 bars of hydrogen pressure. In these conditions small and well-crystallised nanoparticles were obtained. The rhodium nanoparticles synthesised from the precursor $[\text{Rh}(\mu\text{-OMe})(\text{COD})]_2$ were stabilised with PVP (polyvinylpyrrolidone MW= 40000) and diphosphite ligands **1** and **3**, giving rise, respectively, to small and well-crystallised nanoparticles with PVP and large particles with diphosphite ligands. Although further study is required if it is to be determined whether these particles are really large, porous and polycrystalline or whether they consist of small individual nanoparticles, we can conclude that the nature of the metal precursor affects the particles synthesised.

The palladium nanoparticles **Coll.2** and **Coll.3** were used as catalyst in palladium-catalysed allylic alkylation of rac-3-acetoxy-1,3-diphenyl-1-propene with dimethyl malonate. **Colloid.2** system was not stable under catalytic conditions showing not

reproducible results. However, **Colloid.3** system led to an enantiomeric excess of >98%(*S*) in II with high kinetic resolution in the substrate (rac-I) (98% (*S*) in the remaining substrate). This behaviour is similar to that of the previously reported for **Colloid.1**.^[79]

Finally, we studied the use of rhodium nanoparticles, synthesised from [Rh(μ -OMe)(COD)]₂ in the presence of diphosphite ligands **1** and **3** (**Colloid.12** and **Colloid.13**, respectively), as catalyst in the styrene hydroformylation reaction. In both cases the activities were very low. The introduction of an excess of ligand increased the regioselectivity and enantioselectivity. The respective molecular system of **Colloid.12**, **Molecular.12**, and the poisoning test were studied in order to exclude the possible formation of homogeneous catalyst in the colloidal system. The results are difficult to analyse and further analysis are needed to be able to clearly conclude.

4.4 Experimental section

General methods

All syntheses were performed by using standard Schlenk techniques and Fisher-Porter bottle techniques under argon atmosphere. Solvents were purified by standard procedures. Ligands **1**,^[122] **2**,^[123] **3**,^[124] and **4**^[125] were prepared by methods described previously. All other reagents were used as commercially available. ¹H, ¹³C{¹H} and ³¹P{¹H} NMR spectra were recorded on a Varian Gemini 400 MHz spectrometer. Chemical shifts are relative to SiMe₄ (¹H and ¹³C) as internal standard or H₃PO₄ (³¹P) as external standard. All NMR spectral assignments were determined by COSY and HSQC spectra. TEM analysis were prepared by slow evaporation of a drop of each colloidal solution deposited under argon onto a holey carbon-covered copper grid. The TEM experiments were performed at the "Service Commun de Microscopie Electronique de l'Université Paul Sabatier" on a JEOL 200 CX-T electron microscope operating at 200kV and a Philips CM12 electron microscope operating at 120 kV with respective resolutions of 4.5 and 5 Å. The TEM analyses of the nanoparticles after catalysis were performed in the "Servei de Recursos Científics" on a Zeiss 10 CA electron microscope at 100 kV with a

resolution of 3Å. The size distribution of the particles was determined by a manual analysis of enlarged images. At least 150 particles on a given grid were measured in order to obtain a statistical size distribution and a mean diameter. WAXS experiments were mainly performed at CEMES "Centre d'Elaboration des Matériaux et d'Etudes Structurales, CNRS, Toulouse". All samples were sealed in Lindemann glass capillaries. Measurements of the X-ray intensity scattered by the sample irradiated with graphite-monochromatized molybdenum Ka (0.071069 nm) radiation were performed using a dedicated two-axis diffractometer. In order to extract the structure-related component of WAXS, the so-called reduced intensity function(s), then Fourier transformed to allow for radial distribution function (RDF) analysis. Gas chromatographic analyses were run on a Hewlett-Packard HP 5890A instrument (split/splitless injector, J&W Scientific, HP-5, 25 m column, internal diameter 0.25 mm, film thickness 0.33 mm, carrier gas: 150 kPa Ar, F.I.D. detector) equipped with a Hewlett-Packard HP3396 series II integrator. Hydroformylation reactions were carried out in a Parr 450 ml. multiple reaction vessel autoclave. Enantiomeric excesses were measured after oxidation of the aldehydes to the corresponding carboxylic acids on a Hewlett-Packard HP 5890A gas chromatograph (split/splitless injector, J&W Scientific, Supelco β-DEX 110 (30 m. column, internal diameter 0.25 mm., carrier gas: 100 kPa He, F.I.D. detector).

Synthesis of metal precursors

[Ru(C₈H₁₀)(C₈H₁₂)]^[126]

0.34 g (1.3 mmol) of hydrated RuCl₃ was completely dissolved in absolute ethanol (10 ml) under nitrogen. 1,5 cyclooctadiene, previously deoxygenated and filtered through alumina, and zinc dust (3.0 g, 46 mmol) were added and the solution was heated at 80°C for 3 hours. The resulting solution was filtered and the residue was washed with pentane (50 ml). The filtrate was evaporated to dryness under reduced pressure at room temperature and the solid residue obtained was extracted with pentane (2 x 60 ml). The solution was concentrated and passed through alumina using pentane. The yellow pentane solution was concentrated to 5

ml and cooled to -78°C giving 0.20 g of yellow crystals. The resulting highly sensitive yellow crystals were stored under argon at -30°C .

[Rh(μ -OMe)(COD)]₂^[127, 128]

To a solution of [Rh(μ -Cl)(COD)]₂ (175 mg., 0.36 mmol) in dichloromethane (15 ml.) a solution of KOH (40 mg., 0.71 mmol) in methanol (5 ml) was added. Immediately a yellow solid precipitated. After being stirred for 30 minutes at room temperature, the solvent was removed under reduced pressure. Then 10 ml of methanol and subsequently 15 ml of water were added to the residue after which the solid was collected by filtration, and cleaned with water (3 x 5 ml). The solid was dried under reduced pressure over phosphorus (V) oxide and used without further purification.

[Rh(η^3 -C₃H₅)₃]^[129]

To a cold (-10°C) stirred suspension of RhCl₃.H₂O (1.1 g, 5.3 mmol) in THF (93 ml) allylmagnesium chloride (17.5 ml, 2M, 35 mmol) was added dropwise over a period of 10 minutes. The solution slowly lost its yellow-brown color as the RhCl₃.H₂O disappeared over a period of about 1 hour. The solution was then allowed to warm to 10°C and stirred for an additional 16 hours. The THF was removed under reduced pressure and the residue extracted with pentane (3 x 150 ml). The yellow pentane extracted was filtered through celite and the pentane was removed under reduced pressure. The bright yellow residue was transferred to a sublimator and sublimed onto a water-cooled probe over a period of 2 hours using static vacuum (50 - $60^{\circ}\text{C}/10^{-4}$ torr). Yield: 0.8 g (82%)

Synthesis of metal nanoparticles

Synthesis of palladium nanoparticles from the precursor [Pd₂(dba)₃]

In the standard procedure, 160 mg. of palladium precursor [Pd₂(dba)₃] (0.175 mmol) were dissolved under argon at -110°C (ethanol/N₂ bath) in a solution of 160

ml of tetrahydrofuran containing 0.2 equivalents of ligand in a closed pressure bottle. After pressurization at room temperature under 3 bars of hydrogen for 30 minutes, the initial red solution became black in a few minutes. The vigorous magnetic stirring and the hydrogen pressure were maintained for 18 hours. After that period of time, the hydrogen pressure was eliminated, and a drop of the colloidal solution was deposited under argon on a holey carbon covered copper grid for electron microscopy analysis. Precipitation with a tetrahydrofuran/pentane mixture at low temperature gave a black precipitate which was washed with pentane (2x 40 ml) and dried under vacuum. The colloids were characterized by TEM analysis, elemental analysis and WAXS.

Colloid.2 was synthesised according to the standard procedure from 160 mg of $[\text{Pd}_2(\text{dba})_3]$ (0.175 mmol) and 74.7 mg of diphosphite **2** (0.070 mmol) in 160 ml of tetrahydrofuran. The nanoparticles synthesised were analysed by TEM (Transmission electron microscopy), WAXS (Wide-angle X-ray scattering) and elemental analysis. The elemental analysis of the black isolated nanoparticles of **Colloid.2** was 72.97 %Pd, 0.37%P, 13.99%C, 0.38%H.

Colloid.3 was synthesised according to the standard procedure from 160 mg of $[\text{Pd}_2(\text{dba})_3]$ (0.175 mmol) and 106.2 mg of diphosphite **3** (0.070 mmol) in 160 ml of tetrahydrofuran. The nanoparticles synthesised were analysed by TEM (Transmission electron microscopy), WAXS (Wide-angle X-ray scattering) and elemental analysis. The elemental analysis of the black isolated nanoparticles of **Colloid.3** was 68.77 %Pd, 0.33%P, 2.93%Si, 8.82%C, 0.65%H;

Colloid.4 was synthesised according to the standard procedure from 160 mg of $[\text{Pd}_2(\text{dba})_3]$ (0.175 mmol) and 55.7 mg of diphosphite **4** (0.070 mmol) in 160 ml of tetrahydrofuran. The nanoparticles synthesised were analysed by TEM (Transmission electron microscopy), WAXS (Wide-angle X-ray scattering) and elemental analysis. The elemental analysis of the black isolated nanoparticles of **Colloid.4** was 71.59%Pd, 1.97%P, 15.94%C, 1.28%H.

Colloid.5 was synthesised according to the standard procedure from 80 mg of $[\text{Pd}_2(\text{dba})_3]$ (0.088 mmol) and 27.9 mg of diphosphite **4** (0.035 mmol) in 80 ml of

tetrahydrofuran at 60°C. The nanoparticles synthesised were analysed by TEM (Transmission electron microscopy), WAXS (Wide-angle X-ray scattering) and elemental analysis. The elemental analysis of the black isolated nanoparticles of **Colloid.5** was 60.67%Pd, 3.55%P.

Colloid.6 was synthesised according to the standard procedure from 80 mg of $[\text{Pd}_2(\text{dba})_3]$ (0.088 mmol) and 55.7 mg of diphosphite **4** (0.070 mmol) in 80 ml of tetrahydrofuran. The black nanoparticles synthesised did not precipitate and were only analysed by TEM (Transmission electron microscopy).

Synthesis of ruthenium nanoparticles from the precursor

$[\text{Ru}(\text{C}_8\text{H}_{10})(\text{C}_8\text{H}_{12})]$

In the standard procedure 160 mg. of ruthenium precursor $[\text{Ru}(\text{C}_8\text{H}_{10})(\text{C}_8\text{H}_{12})]$ (0.508 mmol) were dissolved under argon at -110°C (ethanol/ N_2 bath) in a solution of 160 ml of tetrahydrofuran containing 0.1 equivalents of ligand in a closed pressure bottle. After pressurization at room temperature under 3 bars of hydrogen for 30 minutes, the initial yellow solution became black in a few minutes. The vigorous magnetic stirring and the hydrogen pressure were maintained for 18 hours. After that period of time, the hydrogen pressure was eliminated, and a drop of the colloidal solution was deposited under argon on a holey carbon covered copper grid for electron microscopy analysis. Precipitation with a tetrahydrofuran/pentane mixture at low temperature gave a black precipitate which was washed with pentane (2x 40 ml) and dried under vacuum. The colloids were characterized by TEM analysis, elemental analysis and WAXS.

Colloid.7 was synthesised according to the standard procedure from 160 mg of $[\text{Ru}(\text{C}_8\text{H}_{10})(\text{C}_8\text{H}_{12})]$ (0.508 mmol) and 54.2 mg of diphosphite **1** (0.051 mmol) in 160 ml of tetrahydrofuran. The nanoparticles synthesised were analysed by TEM (Transmission electron microscopy), WAXS (Wide-angle X-ray scattering) and elemental analysis. The elemental analysis of the black isolated nanoparticles of **Colloid.7** was 42.19%Ru, 1.86%P, 7.72%C, 1.18%H.

Colloid.8 was synthesised according to the standard procedure from 160 mg of $[\text{Ru}(\text{C}_8\text{H}_{10})(\text{C}_8\text{H}_{12})]$ (0.508 mmol) and 77.1 mg of diphosphite **3** (0.051 mmol) in 160 ml of tetrahydrofuran. The elemental analysis of the black isolated nanoparticles of **Colloid.8** was 44.67%Ru, 1.34%P, 2.40%Si, 24.82%C, 2.99%H.

Synthesis of rhodium nanoparticles from the precursor

$[\text{Rh}(\eta^3\text{-C}_3\text{H}_5)_3]$

In the standard procedure 80 mg of rhodium precursor $[\text{Rh}(\eta^3\text{-C}_3\text{H}_5)_3]$ (0.354 mmol) were dissolved under argon at -110°C (ethanol/ N_2 bath) in a solution of 80 ml of tetrahydrofuran containing 0.2 equivalents of ligand in a closed pressure bottle. After pressurization at room temperature under 3 bars of hydrogen for 30 minutes, the initial yellow solution became black in one hour. The vigorous magnetic stirring and the hydrogen pressure were maintained for 18 hours. After that period of time, the hydrogen pressure was eliminated, and a drop of the colloidal solution was deposited under argon on a holey carbon covered copper grid for electron microscopy analysis. Precipitation with a tetrahydrofuran/pentane mixture at low temperature gave a black precipitate which was washed with pentane (2x 40 ml.) and dried under vacuum. The colloids were characterized by TEM analysis, elemental analysis and WAXS.

Colloid.9 was synthesised according to the standard procedure from 80 mg of $[\text{Rh}(\eta^3\text{-C}_3\text{H}_5)_3]$ (0.354 mmol) was 75.5 mg of diphosphite **1** (0.071 mmol) in 80 ml of tetrahydrofuran. The nanoparticles synthesised were analysed by TEM (Transmission electron microscopy), WAXS (Wide-angle X-ray scattering) and elemental analysis. The elemental analysis of the black isolated nanoparticles of **Colloid.9** was 34.23%Rh, 0.61%P, 4.70%C, 0.47%H.

Colloid.10 was synthesised according to the standard procedure from 80 mg of $[\text{Rh}(\eta^3\text{-C}_3\text{H}_5)_3]$ (0.354 mmol) and 107.4 mg of diphosphite **3** (0.071 mmol) in 80 ml of tetrahydrofuran. The nanoparticles synthesised were analysed by TEM (Transmission electron microscopy), WAXS (Wide-angle X-ray scattering) and elemental analysis. The elemental analysis of the black isolated nanoparticles of **Colloid.10** was 37.74%Rh, 2.48%P, 3.88 %Si, 6.79%C, 0.59%H.

Synthesis of rhodium nanoparticles from the precursor [Rh(μ -OMe)(COD)]₂

In the standard procedure 160 mg. of rhodium precursor [Rh(μ -OMe)(COD)]₂ (0.330 mmol) were dissolved under argon at -110°C (ethanol/N₂ bath) in a solution of 160 ml of tetrahydrofuran containing 0.2 equivalents of ligand in a closed pressure bottle. After pressurization at room temperature under 3 bars of hydrogen for 30 minutes, the initial yellow solution became black in a few minutes. The vigorous magnetic stirring and the hydrogen pressure were maintained for 18 hours. After that period of time, the hydrogen pressure was eliminated, and a drop of the colloidal solution was deposited under argon on a holey carbon covered copper grid for electron microscopy analysis. Precipitation with a tetrahydrofuran/pentane mixture at low temperature gave a black precipitate which is washed with pentane (2x 40 ml.) and dried under vacuum. The colloids were characterized by TEM analysis, elemental analysis and WAXS.

Colloid.11. was synthesised according to the standard procedure from 80 mg of [Rh(μ -OMe)(COD)]₂ (0.165 mmol) and 330.4 mg of PVP (polyvinylpyrrolidone MW=40000, Rh/PVP 2.5% weight) in 80 ml of tetrahydrofuran. The nanoparticles synthesised were analysed by TEM (Transmission electron microscopy), WAXS (Wide-angle X-ray scattering) and elemental analysis. The elemental analysis of the grey isolated nanoparticles of **Colloid.11** was 9.31%Rh, 53.71%C, 7.46%H, 9.95%N.

Colloid.12 was synthesised according to the standard procedure from 160 mg of [Rh(μ -OMe)(COD)]₂ (0.331 mmol) and 141.2 mg of diphosphite **1** (0.132 mmol) in 160 ml of tetrahydrofuran. The nanoparticles synthesised were analysed by TEM (Transmission electron microscopy), WAXS (Wide-angle X-ray scattering) and elemental analysis. The elemental analysis of the black isolated nanoparticles of **Colloid.12** was 73.69%Rh, 0.10%P, 2.84%C, 0.10%H.

Colloid.13 was synthesised according to the standard procedure from 160 mg of [Rh(μ -OMe)(COD)]₂ (0.331 mmol) and 200.6 mg of diphosphite **3** (0.132 mmol) in

160 ml of tetrahydrofuran. The nanoparticles synthesised were analysed by TEM (Transmission electron microscopy), WAXS (Wide-angle X-ray scattering) and elemental analysis. The elemental analysis of the black isolated nanoparticles of **Colloid.13** was 16.71%Rh, 0.11%P, 5.24%Si, 4.59%C, 0.38%H.

Hydroformylation experiments

The catalytic precursors were prepared in a multiple reaction vessel autoclave in a glovebox. The experiments with colloidal systems were carried out with 3 mg. nanoparticle, 5.8×10^{-3} mmol of ligand and 5.8 mmol of styrene in 10 ml of toluene. The experiments with molecular systems were carried out from 0.009 mmol of $[\text{Rh}(\text{acac})(\text{CO})_2]$, 0.018 mmol of ligand and 1.8 mmol of styrene in 10 ml of toluene. After pressurising to the desired pressure with syngas and heating the autoclave to the reaction temperature, the reaction mixture was stirred for 24 h. Then the autoclave was cooled to room temperature and depressurised. The reaction mixture was analysed by gas chromatography. The aldehydes obtained from the hydroformylation were oxidised to carboxylic acids to determine the enantiomeric excess.

4.5 References

- [1] G. Schmid, *Chem. Rev.* **1992**, 92, 1709.
- [2] L. N. Lewis, *Chem. Rev.* **1993**, 93, 2693.
- [3] G. Schmid, *Clusters and Colloids: From Theory to Applications* **1994**.
- [4] L. J. De Jongh, *Physics and Chemistry of Metal Cluster Compounds*, Kluwer Academic Publisher, Dordrecht, **1994**.
- [5] K. J. Klabunde, G. Cardenas-Trivino, *Active Metals: Preparation, Characterization, Applications* **1996**, 237.
- [6] N. Toshima, T. Yonezawa, *New J. Chem.* **1998**, 22, 1179.
- [7] L. N. Lewis, *Catalysis by Di- and Polynuclear Metal Cluster Complexes* **1998**, 373.
- [8] K. S. Weddle, J. D. Aiken III, R. G. Finke, *J. Am. Chem. Soc.* **1998**, 120, 5653.
- [9] G. Schmid, M. Bäuml, M. Geerkens, I. Heim, C. Osemann, T. Sawitowski, *Chem. Soc. Rev.* **1999**, 28, 179.
- [10] J. D. Aiken III, R. G. Finke, *J. Mol. Catal. A: Chem.* **1999**, 145, 1.
- [11] M. A. El-Sayed, *Acc. Chem. Res.* **2001**, 34, 257.

- [12] H. Bönnemann, R. M. Richards, *Eur. J. Inorg. Chem.* **2001**, 2455.
- [13] D. L. Feldheim, C. A. Foss Jr., *Metal Nanoparticles* **2002**.
- [14] A. Roucoux, J. Schulz, H. Patin, *Chem. Rev.* **2002**, *102*, 3757.
- [15] J. A. Widegren, R. G. Finke, *J. Mol. Catal. A: Chem.* **2003**, *191*, 187.
- [16] K. Philippot, B. Chaudret, *C. R. Chimie* **2003**, *6*, 1019.
- [17] B. Chaudret, *C. R. Physique* **2005**, *6*, 117.
- [18] T. Graham, *Phil. Trans. Roy. Soc.* **1861**, *151*, 183.
- [19] M. Faraday, *Philos. Trans. R. Soc. London* **1857**, *147*, 145.
- [20] G. Schmid, *Endeavour* **1990**, *14*, 172.
- [21] J. Turkevich, G. Kim, *Science* **1970**, *169*, 873.
- [22] J. Turkevich, P. C. Stevenson, J. Hillier, *Discussions of the Faraday Society* **1951**, 55.
- [23] J. Turkevich, *Gold Bulletin* **1985**, *18*, 86.
- [24] T. Leisner, C. Rosche, S. Wolf, F. Granzer, L. Woste, *Surface Review and Letters* **1996**, *3*, 1105.
- [25] R. Tausch-Treml, A. Henglein, J. Lilie, *Ber. Bunsen-Ges. Phys. Chem.* **1978**, *82*, 1335.
- [26] M. Michaelis, A. Henglein, *J. Phys. Chem.* **1992**, *96*, 4719.
- [27] J. Rothe, J. Hormes, H. Bonnemann, W. Brijoux, K. Siepen, *J. Am. Chem. Soc.* **1998**, *120*, 6019.
- [28] M. A. Watzky, R. G. Finke, *J. Am. Chem. Soc.* **1997**, *119*, 10382.
- [29] J. A. Widegren, J. D. Aiken, S. Ozkar, R. G. Finke, *Chem. Mater.* **2001**, *13*, 312.
- [30] M. A. Watzky, R. G. Finke, *Chem. Mater.* **1997**, *9*, 3083.
- [31] B. J. Hornstein, R. G. Finke, *Chem. Mater.* **2004**, *16*, 139.
- [32] B. J. Hornstein, R. G. Finke, *Chem. Mater.* **2004**, *16*, 3972.
- [33] C. Besson, E. E. Finney, R. G. Finke, *Chem. Mater.* **2005**, *17*, 4925.
- [34] C. Besson, E. E. Finney, R. G. Finke, *J. Am. Chem. Soc.* **2005**, *127*, 8179.
- [35] R. G. Finke, *Metal Nanoparticles: Synthesis, Characterization and Applications*, Marcel Dekkers, New York, **2002**.
- [36] R. J. Hunter, *Foundations of Colloid Science, Vol. 1*, Oxford University Press, New York, **1987**.
- [37] M. E. Labib, *Colloids and Surfaces* **1988**, *29*, 293.
- [38] D. H. Napper, *Polymeric Stabilization of Colloidal Dispersions*, Academic Press, London, **1983**.
- [39] J. D. Aiken III, Y. Lin, R. G. Finke, *J. Mol. Catal. A: Chem.* **1996**, *114*, 29.
- [40] Y. Lin, R. G. Finke, *J. Am. Chem. Soc.* **1994**, *116*, 8335.
- [41] J. Schulz, A. Roucoux, H. Patin, *Chem. Eur. J.* **2000**, *6*, 618.
- [42] V. Mevellec, B. Leger, M. Mauduit, A. Roucoux, *Chem. Commun.* **2005**, 2838.
- [43] K. Esumi, T. Tano, K. Meguro, *Langmuir* **1989**, *5*, 268.

- [44] T. Tano, K. Esumi, K. Meguro, *J. Colloid Interface Sci.* **1989**, *133*, 530.
- [45] J. L. Marignier, J. Belloni, M. O. Delcourt, J. P. Chevalier, *Nature* **1985**, *317*, 344.
- [46] K. Kurihara, J. Kizling, P. Stenius, J. H. Fendler, *J. Am. Chem. Soc.* **1983**, *105*, 2574.
- [47] K. Torigoe, K. Esumi, *Langmuir* **1992**, *8*, 59.
- [48] K. Esumi, A. Suzuki, N. Aihara, K. Usui, K. Torigoe, *Langmuir* **1998**, *14*, 3157.
- [49] K. S. Suslick, M. W. Grinstaff, S.-B. Choe, A. A. Cichowlas, *Nature* **1991**, *353*, 414.
- [50] K. S. Suslick, T. Hyeon, M. Fang, *Chem. Mater.* **1996**, *8*, 2172.
- [51] Y. Kolytyn, G. Katabi, X. Cao, R. Prozorov, A. Gedanken, *Journal of Non-Crystalline Solids* **1996**, *201*, 159.
- [52] M. Andrews, G. A. Ozin, C. G. Francis, *Inorg. Synth.* **1981**, *22*, 116.
- [53] K. J. Klabunde, P. L. Timms, P. S. Skell, S. Ittel, *Inorg. Synth.* **1979**, *19*, 59.
- [54] M. T. Reetz, W. Helbig, *J. Am. Chem. Soc.* **1994**, *116*, 7401.
- [55] M. T. Reetz, S. A. Quaiser, *Angew. Chem. Int. Ed.* **1995**, *34*, 2240.
- [56] M. T. Reetz, W. Helbig, S. A. Quaiser, *Active Metals: Preparation, Characterization, Applications* **1996**, 279.
- [57] P. S. Roberto Giordano, Philippe Kalck, Yolande Kihn, Joachim Schreiber, Christiane Marhic, Jean-Luc Duvail, *European Journal of Inorganic Chemistry* **2003**, *2003*, 610.
- [58] S. Ozkar, R. G. Finke, *J. Am. Chem. Soc.* **2002**, *124*, 5796.
- [59] D. deCaro, T. O. Ely, A. Mari, B. Chaudret, E. Snoeck, M. Respaud, J. M. Broto, A. Fert, *Chem. Mater.* **1996**, *8*, 1987.
- [60] J. S. Bradley, E. W. Hill, S. Behal, C. Klein, B. Chaudret, A. Duteil, *Chem. Mater.* **1992**, *4*, 1234.
- [61] D. De Caro, J. S. Bradley, *New J. Chem.* **1998**, *22*, 1267.
- [62] A. Duteil, R. Quéau, B. Chaudret, R. Mazel, C. Roucau, J. S. Bradley, *Chem. Mater.* **1993**, *5*, 341.
- [63] J. S. Bradley, J. M. Millar, E. W. Hill, S. Behal, B. Chaudret, A. Duteil, *Faraday Discuss.* **1991**, *92*, 255.
- [64] T. O. Ely, C. Amiens, B. Chaudret, E. Snoeck, M. Verelst, M. Respaud, J.-M. Broto, *Chem. Mater.* **1999**, *11*, 526.
- [65] C. Pan, K. Pelzer, K. Philippot, Chaudret, F. Dassenoy, P. Lecante, M.-J. Casanove, *J. Am. Chem. Soc.* **2001**, *123*, 7584.
- [66] O. Vidoni, K. Philippot, C. Amiens, B. Chaudret, O. Balmes, J. Malm, J. Bovin, F. Senocq, M. J. Casanove, *Angew. Chem. Int. Ed.* **1999**, *38*, 3736.
- [67] M. Respaud, J. M. Broto, H. Rakoto, A. R. Fert, L. Thomas, B. Barbara, M. Verelst, E. Snoeck, P. Lecante, A. Mosset, J. Osuna, T. O. Ely, C. Amiens, B. Chaudret, *Phys. Rev. B* **1998**, *57*, 2925.
- [68] M. Respaud, J. M. Broto, H. Rakoto, J. C. Ousset, J. Osuna, T. Ould Ely, C. Amiens, B. Chaudret, S. Askenazy, *Physica B* **1998**, *246-247*, 532.

- [69] E. Ramírez-Meneses, *Synthèse et caractérisation de nanoparticules métalliques à base de Rhodium, Platine et Palladium, stabilisées par des ligands*. **2004**, Laboratoire de Chimie de Coordination du CNRS. (Toulouse).
- [70] D. Wostek-Wojciechowska, J. K. Jeszka, C. Amiens, B. Chaudret, P. Lecante, *J. Colloid Interface Sci.* **2005**, *287*, 107.
- [71] D. Zitoun, M. Respaud, M. C. Fromen, M. J. Casanove, P. Lecante, C. Amiens, B. Chaudret, *Phys. Rev. Lett.* **2002**, *89*.
- [72] F. Dassenoy, M. J. Casanove, P. Lecante, C. Pan, K. Philippot, C. Amiens, B. Chaudret, *Phys. Rev. B* **2001**, *63*.
- [73] F. Dassenoy, K. Philippot, T. Ould-Ely, C. Amiens, P. Lecante, E. Snoeck, A. Mosset, M. J. Casanove, B. Chaudret, *New J. Chem.* **1998**, *22*, 703.
- [74] T. O. Ely, C. Pan, C. Amiens, B. Chaudret, F. Dassenoy, P. Lecante, M. J. Casanove, A. Mosset, M. Respaud, J. M. Broto, *J. Phys. Chem. B* **2000**, *104*, 695.
- [75] C. Pan, F. Dassenoy, M. J. Casanove, K. Philippot, C. Amiens, P. Lecante, A. Mosset, B. Chaudret, *J. Phys. Chem. B* **1999**, *103*, 10098.
- [76] K. Pelzer, O. Vidoni, K. Philippot, B. Chaudret, V. Collière, *Adv. Funct. Mater.* **2003**, *13*, 118.
- [77] E. Ramirez, S. Jansat, K. Philippot, P. Lecante, M. Gomez, A. M. Masdeu-Bulto, B. Chaudret, *J. Organomet. Chem.* **2004**, *689*, 4601.
- [78] M. Gomez, K. Philippot, V. Colliere, P. Lecante, G. Muller, B. Chaudret, *New J. Chem.* **2003**, *27*, 114.
- [79] S. Jansat, M. Gomez, K. Philippot, G. Muller, E. Guiu, C. Claver, S. Castillon, B. Chaudret, *J. Am. Chem. Soc.* **2004**, *126*, 1592.
- [80] J. D. Aiken, R. G. Finke, *J. Am. Chem. Soc.* **1999**, *121*, 8803.
- [81] J. Dupont, G. S. Fonseca, A. P. Umpierre, P. F. P. Fichtner, S. R. Teixeira, *J. Am. Chem. Soc.* **2002**, *124*, 4228.
- [82] J. U. Kohler, J. S. Bradley, *Langmuir* **1998**, *14*, 2730.
- [83] H. Bönemann, G. A. Braun, *Chem. Eur. J.* **1997**, *3*, 1200.
- [84] J. U. Kohler, J. S. Bradley, *Catal. Lett.* **1997**, *45*, 203.
- [85] H. Bönemann, G. A. Braun, *Angew. Chem. Int. Ed.* **1996**, *35*, 1992.
- [86] M. Studer, H. U. Blaser, C. Exner, *Adv. Synth. Catal.* **2003**, *345*, 45.
- [87] X. B. Zuo, H. F. Liu, D. W. Guo, X. Z. Yang, *Tetrahedron* **1999**, *55*, 7787.
- [88] W. Y. Yu, H. F. Liu, Q. Tao, *Chem. Commun.* **1996**, 1773.
- [89] X. L. Yang, Z. L. Deng, H. F. Liu, *J. Mol. Catal. A: Chem.* **1999**, *144*, 123.
- [90] M. H. Liu, W. Y. Yu, H. F. Liu, *J. Mol. Catal. A: Chem.* **1999**, *138*, 295.
- [91] H. Hirai, H. Chawanya, N. Toshima, *Bull. Chem. Soc. Jpn.* **1985**, *58*, 682.
- [92] W. Y. Yu, H. F. Liu, M. H. Liu, Z. J. Liu, *React. Funct. Polym.* **2000**, *44*, 21.
- [93] G. S. Fonseca, J. D. Scholten, J. Dupont, *Synlett* **2004**, 1525.

- [94] J. A. Widegren, R. G. Finke, *Inorg. Chem.* **2002**, *41*, 1558.
- [95] J. Schulz, A. Roucoux, H. Patin, *Chem. Commun.* **1999**, 535.
- [96] A. Roucoux, J. Schulz, H. Patin, *Adv. Synth. Catal.* **2003**, *345*, 222.
- [97] E. Schulz, S. Levigne, A. Roucoux, H. Patin, *Adv. Synth. Catal.* **2002**, *344*, 266.
- [98] V. Mevellec, A. Roucoux, *Inorg. Chim. Acta* **2004**, *357*, 3099.
- [99] V. Mevellec, A. Roucoux, E. Ramirez, K. Philippot, B. Chaudret, *Adv. Synth. Catal.* **2004**, *346*, 72.
- [100] C. W. Scheeren, G. Machado, J. Dupont, P. F. P. Fichtner, S. R. Teixeira, *Inorg. Chem.* **2003**, *42*, 4738.
- [101] C. S. Consorti, F. R. Flores, J. Dupont, *J. Am. Chem. Soc.* **2005**, *127*, 12054.
- [102] E. T. Silveira, A. P. Umpierre, L. M. Rossi, G. Machado, J. Morais, G. V. Soares, I. L. R. Baumvol, S. R. Teixeira, P. F. P. Fichtner, J. Dupont, *Chem. Eur. J.* **2004**, *10*, 3734.
- [103] G. S. Fonseca, A. P. Umpierre, P. F. P. Fichtner, S. R. Teixeira, J. Dupont, *Chem. Eur. J.* **2003**, *9*, 3263.
- [104] M. T. Reetz, G. Lohmer, *Chem. Commun.* **1996**, 1921.
- [105] M. T. Reetz, R. Breinbauer, K. Wanninger, *Tetrahedron Lett.* **1996**, *37*, 4499.
- [106] M. T. Reetz, S. A. Quaiser, C. Merk, *Chem. Ber.* **1996**, *129*, 741.
- [107] M. T. Reetz, R. Breinbauer, P. Wedemann, P. Binger, *Tetrahedron* **1998**, *54*, 1233.
- [108] Y. Li, X. M. Hong, D. M. Collard, M. A. El-Sayed, *Org. Lett.* **2000**, *2*, 2385.
- [109] Y. Li, M. A. El-Sayed, *J. Phys. Chem. B* **2001**, *105*, 8938.
- [110] Y. Li, E. Boone, M. A. El-Sayed, *Langmuir* **2002**, *18*, 4921.
- [111] R. Narayanan, M. A. El-Sayed, *J. Am. Chem. Soc.* **2003**, *125*, 8340.
- [112] R. Narayanan, M. A. El-Sayed, *J. Phys. Chem. B* **2004**, *108*, 8572.
- [113] R. Narayanan, M. A. El-Sayed, *J. Catal.* **2005**, *234*, 348.
- [114] R. Narayanan, M. A. El-Sayed, *Langmuir* **2005**, *21*, 2027.
- [115] R. Narayanan, M. A. El-Sayed, *J. Phys. Chem. B* **2005**, *109*, 12663.
- [116] C. C. Cassol, A. P. Umpierre, G. Machado, S. I. Wolke, J. Dupont, *J. Am. Chem. Soc.* **2005**, *127*, 3298.
- [117] K. Nasar, F. Fache, M. Lemaire, J. C. Beziat, M. Besson, P. Gallezot, *J. Mol. Catal.* **1994**, *87*, 107.
- [118] X. B. Zuo, H. F. Liu, M. H. Liu, *Tetrahedron Lett.* **1998**, *39*, 1941.
- [119] V. Mevellec, C. Mattioda, J. Schulz, J. P. Rolland, A. Roucoux, *J. Catal.* **2004**, *225*, 1.
- [120] Y. L. Huang, J. R. Chen, H. Chen, R. X. Li, Y. Z. Li, L. E. Min, X. J. Li, *J. Mol. Catal. A* **2001**, *170*, 143.
- [121] X. B. Zuo, H. F. Liu, C. Yue, *J. Mol. Catal. A* **1999**, *147*, 63.
- [122] G. J. H. Buisman, M. E. Martin, E. J. Vos, A. Klootwijk, P. C. J. Kamer, P. W. N. M. Van Leeuwen, *Tetrahedron: Asymmetry* **1995**, *6*, 719.

- [123] O. Pamies, G. Net, A. Ruiz, C. Claver, *Tetrahedron; Asymmetry* **1999**, *10*, 2007.
- [124] To be published. See Chapter 2.
- [125] O. Pamies, M. Dieguez, G. Net, A. Ruiz, C. Claver, *Chem. Commun.* **2000**, 2383.
- [126] P. Pertici, G. Vitulli, *Inorg. Synth.* **1983**, *22*, 178.
- [127] M. D. Fryzuk, W. E. Piers, in *Organomet. Synth., Vol. 3* (Eds.: R. B. King, J. J. Eisch), Elsevier, Amsterdam, **1986**, p. 128.
- [128] W. A. Herrmann, in *Synthetic Methods of Organometallic and Inorganic Chemistry* (Ed.: W. A. Herrmann), Stuttgart, **1996**, p. 38.
- [129] R. Uson, L. A. Oro, J. A. Cabeza, *Inorg. Synth.* **1985**, *23*, 126.
- [130] T. D. Ewers, A. K. Sra, B. C. Norris, R. E. Cable, C.-H. Cheng, D. F. Shantz, R. E. Schaak, *Chem. Mater.* **2005**, *17*, 514.
- [131] H. P. Liang, H. M. Zhang, J. S. Hu, Y. G. Guo, L. J. Wan, C. L. Bai, *Angew. Chem. Int. Ed.* **2004**, *43*, 1540.
- [132] G. Schmid, A. Lehnert, J. Malm, J. Bovin, *Angew. Chem. Int. Ed.* **1991**, *30*, 874.
- [133] Y. J. Song, Y. Yang, C. J. Medforth, E. Pereira, A. K. Singh, H. F. Xu, Y. B. Jiang, C. J. Brinker, F. van Swol, J. A. Shelnutt, *J. Am. Chem. Soc.* **2004**, *126*, 635.
- [134] P. W. N. M. van Leeuwen, C. Claver, *Rhodium Catalyzed Hydroformylation, Vol. 22*, Kluwer Academic, **2000**.
- [135] J. A. Widegren, R. G. Finke, *J. Mol. Catal. A: Chem.* **2003**, *198*, 317.